

UPOCR: Towards Unified Pixel-Level OCR Interface

Dezhi Peng^{1,3,*}, Zhenhua Yang^{1,3,*}, Jiaxin Zhang^{1,3}, Chongyu Liu^{1,3}, Yongxin Shi^{1,3},
Kai Ding^{2,3}, Fengjun Guo^{2,3}, Lianwen Jin^{1,3,†}

¹ South China University of Technology, ² INTSIG Information Co. Ltd,

³ INTSIG-SCUT Joint Lab of Document Image Analysis and Recognition

pengdzscut@foxmail.com, eelwjin@scut.edu.cn

Abstract

In recent years, the optical character recognition (OCR) field has been proliferating with plentiful cutting-edge approaches for a wide spectrum of tasks. However, these approaches are task-specifically designed with divergent paradigms, architectures, and training strategies, which significantly increases the complexity of research and maintenance and hinders the fast deployment in applications. To this end, we propose UPOCR, a simple-yet-effective generalist model for Unified Pixel-level OCR interface. Specifically, the UPOCR unifies the paradigm of diverse OCR tasks as image-to-image transformation and the architecture as a vision Transformer (ViT)-based encoder-decoder. Learnable task prompts are introduced to push the general feature representations extracted by the encoder toward task-specific spaces, endowing the decoder with task awareness. Moreover, the model training is uniformly aimed at minimizing the discrepancy between the generated and ground-truth images regardless of the inhomogeneity among tasks. Experiments are conducted on three pixel-level OCR tasks including text removal, text segmentation, and tampered text detection. Without bells and whistles, the experimental results showcase that the proposed method can simultaneously achieve state-of-the-art performance on three tasks with a unified single model, which provides valuable strategies and insights for future research on generalist OCR models. Code will be publicly available.

1. Introduction

Optical character recognition (OCR) is a flourishing field with numerous real-world applications [37, 39, 43, 57, 60], encompassing a wide spectrum of pixel-level tasks that require dense per-pixel predictions, e.g., text removal [25, 40, 55, 59, 84, 95], text segmentation [8, 63, 73, 80, 86, 92], and

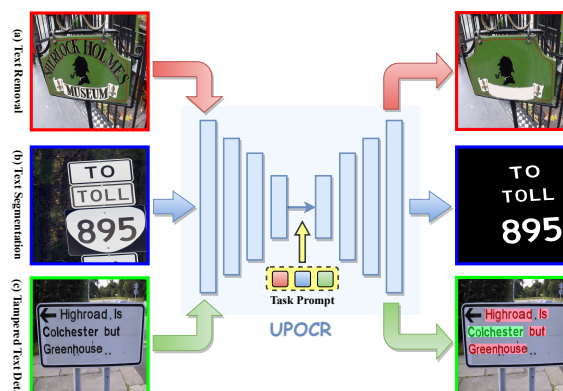


Figure 1. The proposed UPOCR is a unified pixel-level OCR interface which is simultaneously capable of diverse pixel-level OCR tasks (e.g., (a) text removal, (b) text segmentation, and (c) tampered text detection) by prompting ViT-based encoder-decoder. In the bottom-right image, the red and green colors indicate tampered and real texts, respectively.

tampered text detection [50, 62, 82]. Nowadays, there have been massive methods that specialize in individual tasks, significantly contributing to the OCR advancement.

However, specialized OCR models significantly differ in aspects of paradigms, architectures, and training strategies, especially for pixel-level OCR tasks. **(1) Paradigm:** The differences in paradigms are particularly reflected by divergent input and output formats. For instance, existing approaches to text segmentation [86] and tampered text detection [62] typically transform the input image into per-pixel classification probabilities to distinguish text strokes or real/tampered texts from backgrounds. On the contrary, text removal [95] is aimed at producing vivid text-erased images from input images. Moreover, recent studies [36, 41, 84] commonly consolidate text masks into inputs or outputs to promote text perception of text removal models. **(2) Architecture:** Specialized models typically elaborate dedicated modules for individual tasks. Concretely, explicit text localization modules [19, 71] and multi-step refine-

*Equal contribution

†Corresponding author

ments [30, 40, 52, 84] are employed to resolve excessive and inexhaustive text erasure. As for the text segmentation task, advanced methods [8, 63, 80, 86] rely on complex attention and resampling modules as well as semantic information from text recognizers. Moreover, the fusion of frequency and RGB domains is crucial to existing tampered text detection approaches [62, 83]. **(3) Training Strategy:** Specialized models are optimized in disparate manners. In general, the cross-entropy loss is adopted for text segmentation [86, 92] and tampered text detection [62] while L1 distance for text removal [40, 95]. Additionally, abundant dedicated losses are designed for individual tasks, *e.g.*, trimap loss [86, 87] and Lovasz loss [62]. Moreover, several studies [41, 53, 86, 87] incorporate discriminators and GAN-based training strategies. The joint training with text localization modules is another trend in recent studies [73, 84, 92], requiring auxiliary supervision. These inhomogeneities among specialized OCR models raise the research complexity and increase the real-world deployment and maintenance cost. More importantly, the collaboration between OCR tasks cannot be investigated. Therefore, it is urgent to develop generalist pixel-level OCR models.

Concurrently, several studies [5, 13, 49, 76, 79] have been devoted to establishing generalist interfaces. However, OFA [76] and Unified-IO [49] depend on VQGAN [21] to decode images from discrete tokens, thus limiting the diversity and granularity in the pixel space. Although recent approaches [1, 38, 42, 91, 94, 100] investigate the combination of powerful vision Transformers (ViTs) [18, 72] and large language models (LLMs) [69], they struggle with OCR tasks [44, 65] and fail to generate pixels. Painter [79] tackles diverse tasks as inpainting problems but implicitly distinguishes tasks via example pairs, hence difficult to identify OCR tasks with inconspicuous correlation between inputs and outputs. Furthermore, existing generalist OCR models [7, 22, 33, 51, 68, 89, 90] primarily focus on document scenarios and cannot handle pixel-level tasks. In particular, some of them [33, 68] still require dataset-specific finetuning to reach satisfactory performance.

To this end, we propose UPOCR, a simple-yet-effective generalist model for Unified Pixel-level OCR interface. For the first time, UPOCR simultaneously accomplishes multiple pixel-level OCR tasks via prompting ViT-based encoder-decoder as shown in Fig. 1. To achieve this, the proposed method unifies the paradigm, architecture, and training strategy of diverse pixel-level OCR tasks. Specifically, UPOCR unified the paradigm of different tasks as transforming RGB image inputs to RGB image outputs. Moreover, the pure ViT-based encoder-decoder architecture [59] is uniformly adopted for all tasks. To distinguish the ongoing task, we introduce learnable task prompts into the encoder-decoder. Concretely, the encoder first extracts general OCR-related feature representations of the input im-

age. Subsequently, the task prompt pushes the general feature toward the task-specific region, empowering the decoder to generate output images for specific tasks. During training, the model is optimized to minimize the discrepancy between generated and ground-truth (GT) images at pixel and feature levels, eliminating dedicated designs of loss functions, adversarial learning, and auxiliary supervision.

The effectiveness of UPOCR is extensively verified on three pixel-level OCR tasks, including text removal, text segmentation, and tampered text detection. Without bells and whistles, experimental results showcase that UPOCR simultaneously achieves state-of-the-art performance on all three tasks with a unified single model, significantly surpassing specialized methods for individual tasks. In addition, UPOCR outperforms the cutting-edge generalist approach Painter [79] on these three tasks, demonstrating its proficiency in pixel-level OCR field.

In summary, the major contributions are as follows.

- We propose UPOCR, a simple-yet-effective generalist model for unified pixel-level OCR interface. Through the unification of paradigms, architectures, and training strategies, the proposed UPOCR is the first to simultaneously excel in diverse pixel-level OCR tasks.
- Learnable task prompts are introduced to guide the ViT-based encoder-decoder architecture. The prompts push general feature representations from the encoder toward regions of individual tasks, allowing the decoder to perform task-specific decoding.
- The generalist capacity of UPOCR is extensively verified on text removal, text segmentation, and tampered text detection tasks, significantly outperforming existing specialized models. In-depth ablation studies are also conducted to provide valuable strategies and insights for future research on generalist OCR methods.

2. Related Work

2.1. Specialized Pixel-Level OCR Model

Text Removal. Text removal is targeted at replacing text strokes with visually coherent backgrounds, primarily focusing on natural scenes. Early approaches [40, 55, 95] follow a one-stage framework, which implicitly integrates text localization and inpainting processes into a single network in an image-to-image translation manner [27, 54]. However, one-stage approaches struggle with accurate text perception, leaving severe text remnants in text removal results. Therefore, two-stage methods incorporate explicit text segmentation modules [6, 19, 20, 24, 32, 52, 53, 71, 84] or external text detectors [14, 36, 41, 61, 67, 70, 93] for enhanced text localization capacity and have recently dominated the text removal field. Moreover, coarse-to-refine [19, 30, 40, 71] and multi-step progressive refine-

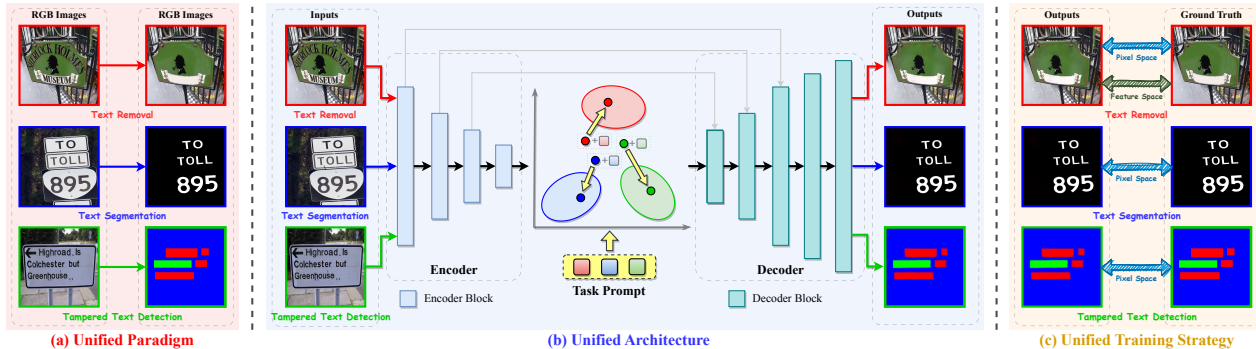


Figure 2. UPOCR is a generalist OCR model which unifies the paradigm, architecture, and training strategy of diverse pixel-level OCR tasks. (a) The paradigm is unified as RGB image to RGB image translation. (b) The ViT-based encoder-decoder architecture is employed for all tasks. Learnable task prompts are inserted to shift general hidden representations to task-specific regions. (c) During training, the model is optimized to minimize the discrepancy between predicted and GT images at pixel and feature spaces.

ments [6, 20, 52, 84] have also been intensively exploited for exhaustive text removal in recent studies. Nevertheless, ViTEraser [59] demonstrated a one-stage framework with ViTs and SegMIM pre-training can significantly outperform previous complicated methods.

Text Segmentation. Text segmentation aims to predict per-pixel classification for distinguishing text strokes from backgrounds. SMANet [8] inserted multi-scale attention into PSPNet [97]-based architecture. TextFormer [80] and ARM-Net [63] further incorporated high-level semantics from text recognizers. Moreover, TexRNet [86] dynamically reactivated low-confidence regions and adopted a character-level discriminator. Based on TexRNet, PGT-SNet [87] additionally integrated a text detector for text-line cropping and employed a line-level discriminator. To fully utilize polygon annotations, Wang *et al.* [73] exploited mutual interaction between polygon- and pixel-level segmentation while Yu *et al.* [92] designed end-to-end hierarchical segmentation Transformers.

Tampered Text Detection. Tampered text detection is defined as the segmentation (or detection) of tampered (or both real and tampered) texts. In the deep learning era, plenty of approaches [4, 17, 34, 35, 98] have been developed for natural image manipulation detection. Inspired by these methods, Qu *et al.* [62] proposed DTD which combines frequency and visual perception for document tampered text detection. Furthermore, Wang *et al.* [83] enhanced Faster R-CNN with RGB and frequency relationship modeling for tampered text detection in receipts. As for natural scenes, Wang *et al.* [82] equipped scene text detectors with the proposed S3R strategy to localize both real and tampered texts.

2.2. Generalist Model

The emergence of Transformer [18, 72] breaks the boundary between different modalities [10, 26, 28, 29, 45, 58, 96], fostering a broad variety of generalist models [75, 88, 101]. One category of these models unifies both the input and

output as sequences and bridges them with a *sequence-to-sequence* learning framework. Pix2Seq [12] pioneered in unifying the output vocabulary of natural language and spatial coordinates and demonstrated effectiveness in object detection. Subsequently, Pix2Seq v2 [13] simultaneously tackled multiple tasks with the guidance of specific prompts. Furthermore, OFA [76] discretized both the input and output as token sequences, accomplishing various unimodal and cross-modal vision-language tasks. Similarly, Unified-IO [49] extended the framework to a wider range of tasks and modalities. With the rise of LLMs [9, 56, 69], numerous studies [1, 38, 42, 91, 94, 100] connected pretrained ViTs and LLMs for generalist models with stronger reasoning and robustness. Following an *image-to-image* translation pipeline, MAE-VQGAN [5] treated diverse tasks as inpainting problems. Painter [79] further investigated visual in-context learning which allows it to adapt to unseen tasks.

In the OCR field, several generalist models have been studied following *sequence-to-sequence* paradigms. Donut [33] pioneered in employing a prompt-based sequence generation framework for document understanding tasks. UDOP [68] further unified the representation of image, text, and layout modalities. Moreover, Nougat [7] and Kosmos-2.5 [51] focused on translating document images into markup languages, encapsulating multiple document OCR tasks into a single sequence. Based on large multimodal models with pretrained ViTs and LLMs, recent approaches [22, 89, 90] augment them using OCR-related data and fine-grained visual perception. However, these approaches primarily focused on document scenarios and failed to generate pixels. Moreover, some of them [33, 68] still required dataset-specific finetuning.

3. Methodology

The proposed UPOCR is a unified pixel-level OCR interface as depicted in Fig. 2. Specifically, UPOCR unifies

the paradigm, architecture, and training strategy of diverse pixel-level OCR tasks. In this paper, the UPOCR is particularly verified on simultaneously handling text removal, text segmentation, and tampered text detection tasks.

3.1. Unified Paradigm

As illustrated in Fig. 2(a), despite their divergent targets (e.g., image generation and segmentation), the paradigm of various pixel-level OCR tasks can be unified to translate RGB images to RGB images. As the inputs are inherently RGB images, detailed output formats of selected tasks are described as follows.

Text Removal. For the text removal task, the output is the text-erased image corresponding to the input, which is also RGB pictures.

Text Segmentation. Text segmentation aims to assign each pixel to foreground (i.e., text stroke) or background. Existing methods typically conduct per-pixel binary classification. However, under the unified image-to-image translation paradigm, UPOCR predicts RGB images with white and black colors. Specifically, the RGB values for foreground and background pixels are (255, 255, 255) and (0, 0, 0), respectively. During inference, the category is determined by thresholding the distance between the generated RGB value and the pre-defined foreground RGB value.

Tampered Text Detection. Following recent studies [82], we define tampered text detection as per-pixel classification of tampered text, real text, and background categories. Similar to text segmentation, we adopt different RGB values in the output image to represent different categories. Concretely, we assign red (255, 0, 0), green (0, 255, 0), and blue (0, 0, 255) colors to tampered texts, real texts, and backgrounds, respectively. During inference, we compare the distance of predicted RGB values with these three colors to determine the per-pixel category.

3.2. Unified Architecture

As shown in Fig. 2(b), we implement the unified image-to-image translation paradigm by prompting a ViT-based encoder-decoder.

Encoder-Decoder. The encoder-decoder architecture is inspired by ViTEraser [59] which achieves significant success in the text removal field. Specifically, the encoder consists of four sequential blocks, yielding four feature maps with strides of {4, 8, 16, 32} w.r.t the input image. Each encoder block encapsulates a patch embedding layer for downsampling and Swin Transformer v2 blocks [47]. Subsequently, the decoder hierarchically upsamples the final feature of the encoder to strides of {16, 8, 4, 2, 1} w.r.t the input size through five blocks. Each decoder block concatenates Swin Transformer v2 blocks [47] and a patch splitting layer for upsampling. Based on the final feature of the decoder, the output image is predicted using a 3×3 convolution.

Task Prompt. To effectively handle multiple tasks, we introduce learnable task prompts into the encoder-decoder architecture. Retrospectively, recent generalist models [13, 33, 51, 68] prepend task prompts comprising natural language or pre-defined tokens to the decoder for task-specific sequence generation. In contrast, we insert learnable task prompts into the shared feature space of the encoder and decoder as shown in Fig. 2(b). Specifically, for each task, its prompt is formulated as a learnable embedding with the same dimension as the hidden feature from the encoder. To perform a certain task, the corresponding prompt is simply added to every pixel of the hidden feature, pushing the general OCR-related presentations generated by the encoder toward the task-specific region. Subsequently, the decoder translates the adjusted hidden feature to the output image for this specific task. With negligible parameter and computation overhead, the UPOCR can simultaneously deal with diverse tasks in a simple yet effective fashion.

3.3. Unified Training Strategy

Thanks to the unified image-to-image paradigm, the training of UPOCR consistently aims to minimize the discrepancy between the generated and GT images at pixel and feature spaces regardless of the inhomogeneity among tasks, as shown in Fig. 2(c). For conciseness, we define the input, output, and GT images as I_{in} , I_{out} , and I_{gt} , respectively.

Pixel Space. The discrepancy in pixel space is measured by the L1 distance between output and GT images. Furthermore, a multi-scale L1 loss is involved to enhance the perception at multiple granularities during training. Specifically, multi-scale images $I_{out}^{\frac{1}{4}}$ and $I_{out}^{\frac{1}{2}}$ are predicted based on the features from the 3rd and 4th decode blocks, each through a 3×3 convolution. Denoting $\mathbb{I}_{out} = \{I_{out}^{\frac{1}{4}}, I_{out}^{\frac{1}{2}}, I_{out}\}$ and $\mathbb{I}_{gt} = \{I_{gt}^{\frac{1}{4}}, I_{gt}^{\frac{1}{2}}, I_{gt}\}$ ($I_{gt}^{\frac{1}{4}}$ and $I_{gt}^{\frac{1}{2}}$ is resized from I_{gt}), the pixel loss is formulated as:

$$L_{pix} = \sum_{i=1}^3 \alpha_i \|\mathbb{I}_{out}^i - \mathbb{I}_{gt}^i\|_1, \quad (1)$$

where the balancing factor α is empirically set to {5, 6, 10}.

Feature Space. For tasks associated with realistic image generation, the similarity at high-level feature space is critical. Therefore, we additionally align the output and GT images at the feature space for the text removal task. The feature loss L_{feat} is composed of perceptual loss L_{per} [31] and style loss L_{sty} [23]:

$$L_{feat} = 0.01 \times L_{per} + 120 \times L_{sty}, \quad (2)$$

where L_{per} and L_{sty} are calculated following previous studies [40, 41, 59] using a pretrained VGG-16 [66] network.

Total Loss. The total loss L_{total} is the sum of pixel loss L_{pix} and feature loss L_{feat} (if applicable):

$$L_{total} = L_{pix} + L_{feat}. \quad (3)$$

Prompt Insert Position			Text Removal				Text Segmentation		Tampered Text Det.	
Encoder	Shared Feature	Decoder	PSNR \uparrow	MSSIM \uparrow	MSE \downarrow	FID \downarrow	fgIoU \uparrow	F \uparrow	mIoU \uparrow	mF \uparrow
✓	✓		36.93	97.64	0.0430	10.45	88.61	93.96	70.19	82.48
	✓	✓	<u>36.96</u>	97.64	0.0428	<u>10.46</u>	<u>88.78</u>	<u>94.06</u>	71.13	83.13
✓	✓	✓	36.86	97.64	0.0436	10.55	88.84	94.09	<u>71.40</u>	83.31
	✓		37.14	<u>97.62</u>	0.0428	10.47	88.76	94.04	71.71	83.53

Table 1. Ablation study on the insertion of task prompts. The **bold** and underline indicate the best and second best, respectively.

Initialization	Text Removal				Text Segmentation		Tampered Text Det.	
	PSNR \uparrow	MSSIM \uparrow	MSE \downarrow	FID \downarrow	fgIoU \uparrow	F \uparrow	mIoU \uparrow	mF \uparrow
ImageNet	35.67	<u>96.86</u>	0.3556	12.76	86.53	92.78	47.96	64.80
SegMIM	37.04	97.62	<u>0.0433</u>	10.64	<u>88.53</u>	<u>93.92</u>	73.62	84.80
ViTEraser	37.14	97.62	0.0428	10.47	88.76	94.04	<u>71.71</u>	<u>83.53</u>

Table 2. Ablation study on different weight initializations during training.

4. Experiment

4.1. Experiment Setting

Task and Dataset. We investigate three pixel-level OCR tasks, including text removal, text segmentation, and tampered text detection, to demonstrate the effectiveness of UPOCR on generalist pixel-level OCR processing. The SCUT-EnsText [40], TextSeg [86], and Tampered-IC13 [82] datasets are employed for these three tasks, respectively.

Network Architecture. The network architecture of UPOCR inherits from ViTEraser-Small [59] but incorporates three learnable prompts for multi-task processing, totally containing 108M parameters. During training, the weights of UPOCR are initialized from the pretrained ViTEraser-Small (with SegMIM pre-training). The input size is set to 512×512 .

Other Details. See the supplementary material for implementation and inference details.

4.2. Evaluation Metrics

Text Removal. Following previous methods [40, 41], the evaluation for text removal involves image- and detection-eval metrics. The image-eval metrics include PSNR, MSSIM, MSE, AGE, pEPs, pCEPs, and FID while the detection-eval metrics are precision (P), recall (R), and f-measure (F) using the pretrained text detector CRAFT [2]. Note that MSSIM and MSE are presented in percent (%).

Text Segmentation. The intersection over union (IoU), P, R, and F of foreground pixels are employed for evaluation on text segmentation [86].

Tampered Text Detection. Similar to [82], we calculate the P, R, F, and IoU of both real and tampered pixels. We especially focus on the mean f-measure (mF) and mean IoU (mIoU) of real and tampered pixels for overall evaluation.

4.3. Ablation Study

Insertion of Task Prompts. The crucial component of the generalist proficiency of UPOCR is the learnable task prompt. As specified in Sec. 3.2 and Fig. 2(b), the task prompt is inserted to the shared feature space between the encoder and decoder, following the idea that the encoder extracts versatile OCR-related features and the decoder decodes task-specific output images from adjusted hidden features. Nevertheless, the task prompts can also be inserted into the intermediate features of the encoder and decoder, after each encoder block and decoder block. In Tab. 1, we investigate different inserting positions of task prompts. If task prompts are supposed to be integrated into the encoder or decoder, they will go through linear layers to match the required dimensions of intermediate features. The experimental results suggest simply inserting task prompts into the shared feature space can effectively prompt the decoder to generate images for specific tasks. Moreover, it also brings extremely small overhead on parameters (2.3K) and computational costs (only an element-wise addition to a $16 \times 16 \times 768$ feature map).

Weight Initialization. Retrospectively, existing generalist models [1, 38, 42, 51, 100] mostly rely on pretrained weights from strong vision or language models. As described in Sec. 4.1, UPOCR uses the pretrained ViTEraser (with SegMIM pre-training) [59] for initialization during training. In Tab. 2, other two ways of weight initialization are investigated, including *ImageNet* and *SegMIM*. Specifically, for *ImageNet* manner, a Swin Transformer v2 [47] pretrained on the ImageNet-1k [16] classification task is adopted to initialize the encoder, while for *SegMIM* manner, pretrained weights using SegMIM [59] are employed to initialize the encoder-decoder. It can be seen that the initialization is critical to the generalist model performance. The *SegMIM* and *ViTEraser* pretrained weights may effectively learn the essential capacity to grasp text shapes and textures as well as the distinctive features between texts and back-

TR	TS	TTD	Text Removal				Text Segmentation		Tampered Text Det.	
			PSNR \uparrow	MSSIM \uparrow	MSE \downarrow	FID \downarrow	fgIoU \uparrow	F \uparrow	mIoU \uparrow	mF \uparrow
✓			36.97	97.57	0.0500	10.50	-	-	-	-
	✓		-	-	-	-	<u>88.83</u>	<u>94.08</u>	-	-
		✓	-	-	-	-	-	-	67.73	80.72
✓	✓		36.91	97.64	<u>0.0450</u>	10.40	88.64	93.98	-	-
		✓	-	-	-	-	89.07	94.22	<u>70.78</u>	<u>82.89</u>
✓		✓	<u>37.08</u>	97.60	0.0452	<u>10.47</u>	-	-	69.26	81.83
✓	✓	✓	37.14	<u>97.62</u>	0.0428	<u>10.47</u>	88.76	94.04	71.71	83.53

Table 3. Ablation study on task collaboration. (TR: text removal, TS: text segmentation, TTD: tampered text detection)

Method	Venue	Image-Eval							Detection-Eval		
		PSNR \uparrow	MSSIM \uparrow	MSE \downarrow	AGE \downarrow	pEPs \downarrow	pCEPs \downarrow	FID \downarrow	R \downarrow	P \downarrow	F \downarrow
Original	-	-	-	-	-	-	-	-	69.5	79.4	74.1
Pix2pix [27]	CVPR'17	26.70	88.56	0.37	6.09	0.0480	0.0227	46.88	35.4	69.7	47.0
STE [55]	ICDAR'17	25.47	90.14	0.47	6.01	0.0533	0.0296	43.39	5.9	40.9	10.2
EnsNet [95]	AAAI'19	29.54	92.74	0.24	4.16	0.0307	0.0136	32.71	32.8	68.7	44.4
MTRNet++ [71]	CVIU'20	29.63	93.71	0.28	3.51	0.0305	0.0168	35.68	15.1	63.8	24.4
EraseNet [40]	TIP'20	32.30	95.42	0.15	3.02	0.0160	0.0090	19.27	4.6	53.2	8.5
SSTE [67]	TIP'21	35.34	96.24	0.09	-	-	-	-	3.6	-	-
PSSTRNet [52]	ICME'22	34.65	96.75	0.14	<u>1.72</u>	0.0135	0.0074	-	5.1	47.7	9.3
CTRNet [41]	ECCV'22	35.20	97.36	0.09	2.20	0.0106	0.0068	13.99	1.4	38.4	2.7
GaRNet [36]	ECCV'22	35.45	97.14	0.08	1.90	0.0105	0.0062	15.50	1.6	42.0	3.0
MBE [24]	ACCV'22	35.03	97.31	-	2.06	0.0128	0.0088	-	-	-	-
PEN [20]	CVIU'22	35.72	96.68	0.05	1.95	0.0071	0.0020	-	2.1	26.2	3.9
PERT [84]	TIP'23	33.62	97.00	0.13	2.19	0.0135	0.0088	-	4.1	50.5	7.6
SAEN [19]	WACV'23	34.75	96.53	0.07	1.98	0.0125	0.0073	-	-	-	-
FETNet [53]	PR'23	34.53	97.01	0.13	1.75	0.0137	0.0080	-	5.8	51.3	10.5
ViTEraser-Base [59]	-	<u>37.11</u>	<u>97.61</u>	<u>0.0474</u>	1.70	<u>0.0066</u>	<u>0.0035</u>	10.15	0.389	<u>29.7</u>	0.768
UPOCR	-	37.14	97.62	0.0428	<u>1.72</u>	0.0064	0.0034	<u>10.47</u>	<u>0.614</u>	36.6	<u>1.208</u>

Table 4. Comparison with **specialized** models for text removal on the SCUT-EnsText dataset. For a fair comparison, MTRNet++ uses empty coarse masks and GaRNet uses text masks from pretrained CRAFT [2] instead of leveraging GT text masks.

grounds. Therefore, the UPOCR can be rapidly adapted to various pixel-level OCR tasks with superior performance. Although the *SegMIM* is also an effective pre-training approach for UPOCR, we opt for the *ViTEraser* pretrained weights due to the better performance on two of the three tasks.

Task Collaboration. In Tab. 3, we conduct the experiments with different task compositions. Based on these results, We come to the following insights. (1) *The task with insufficient samples can easily benefit from the joint training with other tasks.* For example, the Tampered-IC13 [82] dataset used for tampered text detection contains only 229 training samples, which is inadequate to train a network with 108M parameters despite effective pre-training weights. Therefore, the performance of tampered text detection is consistently improved because the fundamental text localization capacity can be boosted by other tasks. (2) *The joint training of tasks leads to mutual collaboration if with similar targets but negative effect if with exclusive targets.* For instance, text removal aims at erasing the texts while text segmentation needs to highlight them at a fine-grained stroke level. Therefore, additional text removal task always leads to downgraded text segmentation performance. However, comparing the 2nd and 5th rows, tampered text detection

Method	Venue	fgIoU \uparrow	P \uparrow	R \uparrow	F \uparrow
U-Net [64]	MICCAI'15	-	89.00	77.40	82.80
DeepLabV3+ [11]	ECCV'18	84.07	-	-	91.40
HRNetv2-W48 [74]	TPAMI'20	85.03	-	-	91.40
HRNetv2-W48+OCR [74]	TPAMI'20	85.98	-	-	91.80
TexRNet+DeepLabV3+ [86]	CVPR'21	86.06	-	-	92.10
TexRNet+HRNetv2-W48 [86]	CVPR'21	86.84	-	-	92.40
SegFormer [85]	NeurIPS'21	84.59	-	-	91.60
ARM-Net [63]	ACCV'22	-	<u>92.80</u>	<u>92.60</u>	92.70
TFT [92]	ACM MM'23	<u>87.11</u>	-	-	<u>93.10</u>
UPOCR	-	88.76	94.55	93.55	94.04

Table 5. Comparison with **specialized** models for text segmentation on the TextSeg dataset. The performances of U-Net and SegFormer are cited from [63] and [92], respectively.

helps improve the accuracy of text segmentation, because the former provides auxiliary polygon-level text location supervision. Due to the large model capacity, the final model can achieve a good balance of three tasks.

4.4. Comparison with Specialized Models

The comparisons of UPOCR with existing specialized methods for text removal, text segmentation, and tampered text detection are presented in Tabs. 4, 5, and 6, respectively. Furthermore, the visualization results on three tasks are shown in Fig. 3. Without bells and whistles, the

Method	Venue	Real Text				Tampered Text				mIoU \uparrow	mF \uparrow
		IoU \uparrow	P \uparrow	R \uparrow	F \uparrow	IoU \uparrow	P \uparrow	R \uparrow	F \uparrow		
Detection-based Methods											
S3R [82]+EAST [99]	ECCV'22	-	50.46	27.32	35.45	-	70.23	69.97	69.94	-	52.70
S3R [82]+PSENet [77]	ECCV'22	-	61.56	41.89	49.85	-	79.92	79.43	79.67	-	64.76
S3R [82]+ContourNet [81]	ECCV'22	-	77.88	54.80	64.33	-	86.68	91.45	88.99	-	76.66
S3R [82]+ATTR [78]	ECCV'22	-	76.74	54.63	63.83	-	84.60	<u>90.63</u>	<u>87.52</u>	-	75.68
Segmentation-based Methods											
CAT-Net [35]	IJCV'22	-	-	-	-	28.31	31.45	73.91	44.13	-	-
DeepLabV3+ [11]	ECCV'18	48.12	79.83	54.78	64.98	72.21	89.75	78.71	83.86	60.17	74.42
HRNetv2 [74]	TPAMI'20	43.26	76.35	49.95	60.39	73.12	<u>89.98</u>	79.60	84.47	58.19	72.43
BEiT-Uper [3]	ICLR'22	57.07	81.23	65.74	72.67	70.88	82.27	83.66	82.96	63.98	77.82
SegFormer [85]	NeurIPS'21	53.22	86.39	58.09	69.47	77.78	91.78	83.60	87.50	65.50	78.49
Swin-Uper [46]	ICCV'21	<u>61.82</u>	<u>87.82</u>	<u>67.62</u>	<u>76.41</u>	<u>77.28</u>	89.67	84.83	87.18	<u>69.55</u>	<u>81.80</u>
UPOCR	-	71.80	93.31	75.70	83.59	71.62	79.76	87.53	83.46	71.71	83.53

Table 6. Comparison with **specialized** models for tampered text detection on the Tampered-IC13 dataset. CAT-Net can only perform binary classification between tampered texts and backgrounds.

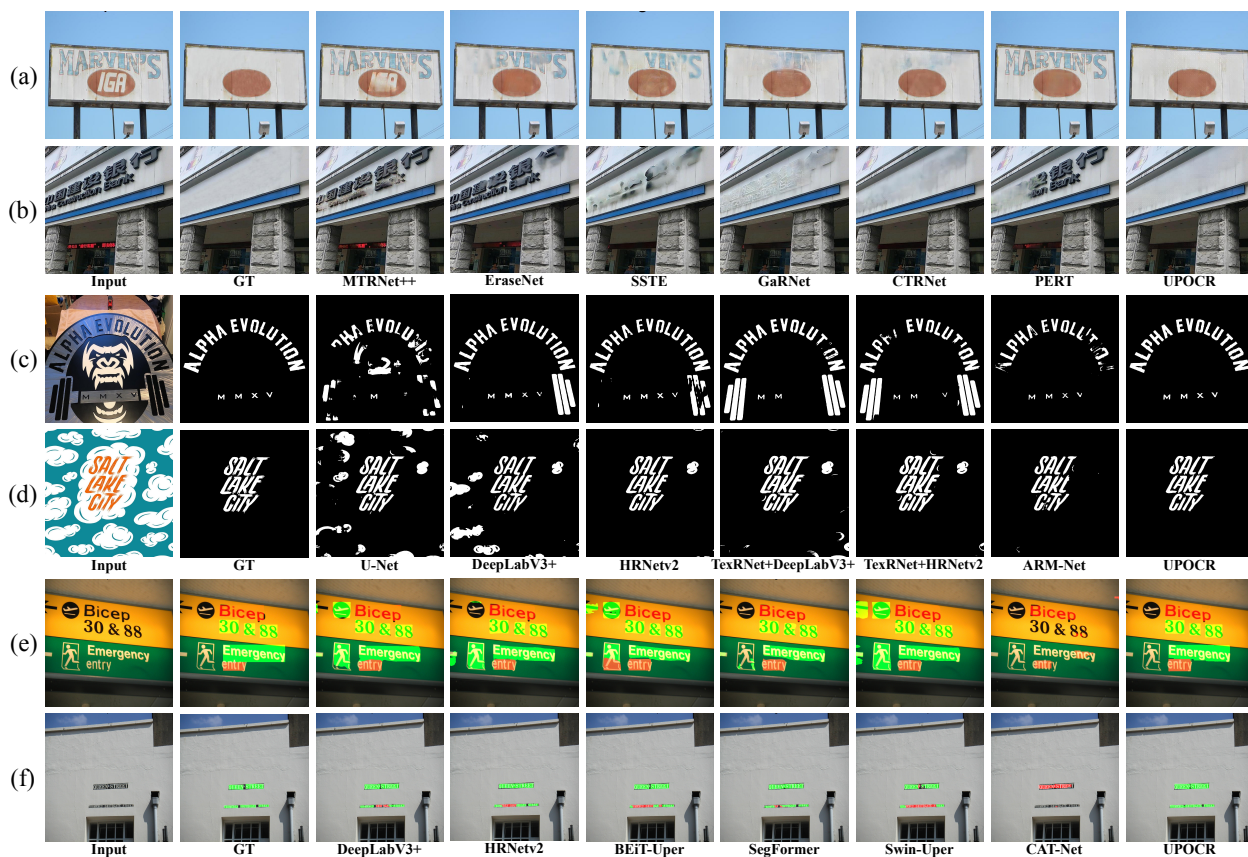


Figure 3. Qualitative comparison of UPOCR and existing **specialized** models on (a)-(b) text removal, (c)-(d) text segmentation, and (e)-(f) tampered text detection (red: tampered, green: real). Zoom in for a better view.

generalist UPOCR with shared parameters can simultaneously outperform existing specialized models for individual tasks. (1) *Text Removal*: The UPOCR eschews the complicated text localization modules, external text detectors, and multi-step refinements. Furthermore, UPOCR discards the GAN-based training strategy and mask branch of ViT-Eraser during training. Following a concise pipeline, UP-

OCR achieves state-of-the-art image-eval performance on SCUT-EnsText [40], outperforming ViTEraser-Base [59] with a ViTEraser-Small model size. As for detection-eval metrics, the 0.614% recall of UPOCR is comparable to ViTEraser, demonstrating nearly all texts are exhaustively erased. It is worth noting that compared with earlier approaches, UPOCR significantly outperforms them in terms

Method	Venue	Text Removal							Text Segmentation				Tampered Text Det.	
		PSNR \uparrow	MSSIM \uparrow	MSE \downarrow	AGE \downarrow	pEPs \downarrow	pCEPs \downarrow	FID \downarrow	fgIoU \uparrow	P \uparrow	R \uparrow	F \uparrow	mIoU \uparrow	mF \uparrow
Painter [79]	CVPR'23	27.13	91.67	0.2942	8.68	0.0898	0.0425	21.90	86.36	93.40	91.97	92.68	69.26	81.83
UPOCR	-	37.14	97.62	0.0428	1.72	0.0064	0.0034	10.47	88.76	94.55	93.55	94.04	71.71	83.53

Table 7. Comparison with generalist models (Painter) on pixel-level OCR tasks.



Figure 4. Qualitative comparison of UPOCR and Painter on (a) text removal, (b) text segmentation, and (c) tampered text detection (red: tampered, green: real). Zoom in for a better view.

of both image- and detection-eval metrics. (2) *Text Segmentation*. Although previous methods utilize attentive modules for refinements, text detectors for coarse text localization, and text recognizers for semantic supervision, UPOCR significantly outperforms them on TextSeg [86] using a single encoder-decoder without extra modules and annotations. (3) *Tampered Text Detection*. The UPOCR achieves the best performance of 71.71% mIoU and 83.53% mF on Tampered-IC13 [82], eliminating the need for frequency domain fusion [35, 62, 83] and adaptation based on text detectors [82]. Note that the segmentation-based methods are reimplemented using MMSegmentation [15] and CAT-Net’s official codes¹.

4.5. Comparison with Generalist Models

To demonstrate the effectiveness of UPOCR over existing generalist models, we re-train Painter [79] using the official implementation² and the same dataset as ours. The performances of UPOCR and Painter are listed in Tab. 7 while the visualizations are illustrated in Fig. 4. Because Painter learns the task target from an example input-output pair, it may hardly grasp the inconspicuous correlation such as tiny text erasing (Fig. 4(a)) and a strong ability to distinguish texts from text-like patterns (Fig. 4(c)). Moreover, as the image is predicted through inpainting, the output cannot guarantee consistent colors as inputs, e.g., red vs. orange

¹<https://github.com/mjkwon2021/CAT-Net>

²<https://github.com/baaivision/Painter>

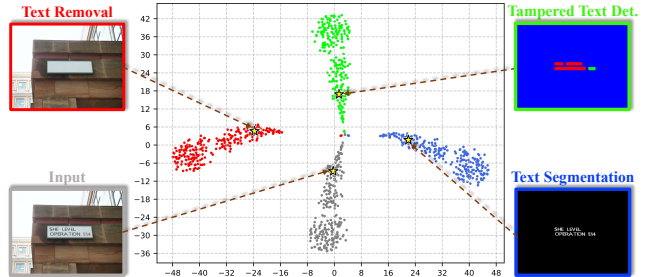


Figure 5. The t-SNE visualization of general features (gray circles) extracted by the encoder and task-specific features integrated with task prompts. Red, green and blue circles are for text removal, tampered text detection, and text segmentation, respectively. The example input image and three-task outputs are visualized along with corresponding features (yellow stars).

walls in Fig. 4(a). Therefore, UPOCR surpasses Painter on all three tasks, especially the text removal task.

4.6. Interpretability of Task Prompts

To investigate the mechanism of task prompts, we visualize the features before and after integrated with task prompts in Fig. 5. Specifically, we perform all three tasks on the 233 testing samples of Tampered-IC13 [82] using corresponding task prompts. We can observe that there are clear boundaries between the general features (gray circles) extracted by the encoder and the task-specific features (red, green, and blue circles), indicating the proposed task prompts can effectively adapt the general features into task-specific regions to generate output images for individual tasks.

5. Conclusion

In this paper, we propose UPOCR, a first-of-its-kind simple-yet-effective unified pixel-level OCR interface. To acquire generalist capability, UPOCR unifies the paradigm, architecture, and training strategies of diverse pixel-level OCR tasks. Specifically, existing divergent paradigms are unified as RGB image to RGB image transformation. To implement this paradigm, UPOCR uniformly adopts a ViT-based encoder-decoder with learnable task prompts to handle various tasks. During training, the strategy is unified to minimize the discrepancy between the generated and ground-truth images at pixel and feature spaces. Extensive experiments are conducted on text removal, text segmentation, and tampered text detection to verify the generalist profi-

ciency of UPOCR. The experimental results demonstrate that UPOCR simultaneously achieves state-of-the-art performance with shared parameters, significantly surpassing specialized OCR models. Comprehensive ablation studies and visual analyses are also presented to provide in-depth insights. We believe this work could be extended to broader tasks and spark more research on generalist OCR models.

References

- [1] Jean-Baptiste Alayrac, Jeff Donahue, Pauline Luc, Antoine Miech, Iain Barr, Yana Hasson, Karel Lenc, Arthur Mensch, Katherine Millican, Malcolm Reynolds, et al. Flamingo: A visual language model for few-shot learning. *Proc. Adv. Neural Inf. Process. Syst. (NeurIPS)*, 35:23716–23736, 2022. [2](#), [3](#), [5](#)
- [2] Youngmin Baek, Bado Lee, Dongyoon Han, Sangdoon Yun, and Hwalsuk Lee. Character region awareness for text detection. In *Proc. IEEE Conf. Comput. Vis. Pattern Recog. (CVPR)*, pages 9365–9374, 2019. [5](#), [6](#)
- [3] Hangbo Bao, Li Dong, Songhao Piao, and Furu Wei. BEiT: BERT pre-training of image Transformers. In *Proc. Int. Conf. Learn. Represent. (ICLR)*, 2022. [7](#), [19](#)
- [4] Jawadul H Bappy, Cody Simons, Lakshmanan Nataraj, BS Manjunath, and Amit K Roy-Chowdhury. Hybrid LSTM and encoder–decoder architecture for detection of image forgeries. *IEEE Trans. Image Process.*, 28(7):3286–3300, 2019. [3](#)
- [5] Amir Bar, Yossi Gandelsman, Trevor Darrell, Amir Globerson, and Alexei Efros. Visual prompting via image inpainting. *Proc. Adv. Neural Inf. Process. Syst. (NeurIPS)*, 35: 25005–25017, 2022. [2](#), [3](#)
- [6] Xuewei Bian, Chaoqun Wang, Weize Quan, Juntao Ye, Xiaopeng Zhang, and Dong-Ming Yan. Scene text removal via cascaded text stroke detection and erasing. *Comput. Vis. Media*, 8:273–287, 2022. [2](#), [3](#)
- [7] Lukas Blecher, Guillem Cucurull, Thomas Scialom, and Robert Stojnic. Nougat: Neural optical understanding for academic documents. *arXiv preprint arXiv:2308.13418*, 2023. [2](#), [3](#)
- [8] Simone Bonechi, Monica Bianchini, Franco Scarselli, and Paolo Andreini. Weak supervision for generating pixel-level annotations in scene text segmentation. *Pattern Recognit. Lett.*, 138:1–7, 2020. [1](#), [2](#), [3](#)
- [9] Tom Brown, Benjamin Mann, Nick Ryder, Melanie Subbiah, Jared D Kaplan, Prafulla Dhariwal, Arvind Neelakantan, Pranav Shyam, Girish Sastry, Amanda Askell, et al. Language models are few-shot learners. *Proc. Adv. Neural Inf. Process. Syst. (NeurIPS)*, 33:1877–1901, 2020. [3](#)
- [10] Nicolas Carion, Francisco Massa, Gabriel Synnaeve, Nicolas Usunier, Alexander Kirillov, and Sergey Zagoruyko. End-to-end object detection with Transformers. In *Proc. Eur. Conf. Comput. Vis. (ECCV)*, pages 213–229, 2020. [3](#)
- [11] Liang-Chieh Chen, Yukun Zhu, George Papandreou, Florian Schroff, and Hartwig Adam. Encoder-decoder with atrous separable convolution for semantic image segmentation. In *Proc. Eur. Conf. Comput. Vis. (ECCV)*, pages 801–818, 2018. [6](#), [7](#), [18](#), [19](#)
- [12] Ting Chen, Saurabh Saxena, Lala Li, David J Fleet, and Geoffrey Hinton. Pix2Seq: A language modeling framework for object detection. In *Proc. Int. Conf. Learn. Represent. (ICLR)*, 2021. [3](#)
- [13] Ting Chen, Saurabh Saxena, Lala Li, Tsung-Yi Lin, David J Fleet, and Geoffrey E Hinton. A unified sequence interface for vision tasks. *Proc. Adv. Neural Inf. Process. Syst. (NeurIPS)*, 35:31333–31346, 2022. [2](#), [3](#), [4](#)
- [14] Benjamin Conrad and Pei-I Chen. Two-stage seamless text erasing on real-world scene images. In *Proc. IEEE Int. Conf. Image Process. (ICIP)*, pages 1309–1313, 2021. [2](#)
- [15] MMSegmentation Contributors. MMSegmentation: Openmmlab semantic segmentation toolbox and benchmark. <https://github.com/open-mmlab/mms Segmentation>, 2020. [8](#)
- [16] Jia Deng, Wei Dong, Richard Socher, Li-Jia Li, Kai Li, and Li Fei-Fei. ImageNet: A large-scale hierarchical image database. In *Proc. IEEE Conf. Comput. Vis. Pattern Recog. (CVPR)*, pages 248–255, 2009. [5](#), [14](#)
- [17] Chengbo Dong, Xinru Chen, Ruohan Hu, Juan Cao, and Xirong Li. MVSS-Net: Multi-view multi-scale supervised networks for image manipulation detection. *IEEE Trans. Pattern Anal. Mach. Intell.*, 45(3):3539–3553, 2022. [3](#)
- [18] Alexey Dosovitskiy, Lucas Beyer, Alexander Kolesnikov, Dirk Weissenborn, Xiaohua Zhai, Thomas Unterthiner, Mostafa Dehghani, Matthias Minderer, Georg Heigold, Sylvain Gelly, et al. An image is worth 16x16 words: Transformers for image recognition at scale. In *Proc. Int. Conf. Learn. Represent. (ICLR)*, 2021. [2](#), [3](#)
- [19] Xiangcheng Du, Zhao Zhou, Yingbin Zheng, Tianlong Ma, Xingjiao Wu, and Cheng Jin. Modeling stroke mask for end-to-end text erasing. In *Proc. IEEE Winter Conf. Appl. Comput. Vis. (WACV)*, pages 6151–6159, 2023. [1](#), [2](#), [6](#)
- [20] Xiangcheng Du, Zhao Zhou, Yingbin Zheng, Xingjiao Wu, Tianlong Ma, and Cheng Jin. Progressive scene text erasing with self-supervision. *Comput. Vis. Image Underst.*, 233: 103712, 2023. [2](#), [3](#), [6](#)
- [21] Patrick Esser, Robin Rombach, and Bjorn Ommer. Taming Transformers for high-resolution image synthesis. In *Proc. IEEE Conf. Comput. Vis. Pattern Recog. (CVPR)*, pages 12873–12883, 2021. [2](#), [15](#)
- [22] Hao Feng, Zijian Wang, Jingqun Tang, Jinghui Lu, Wengang Zhou, Houqiang Li, and Can Huang. UniDoc: A universal large multimodal model for simultaneous text detection, recognition, spotting and understanding. *arXiv preprint arXiv:2308.11592*, 2023. [2](#), [3](#)
- [23] Leon A Gatys, Alexander S Ecker, and Matthias Bethge. Image style transfer using convolutional neural networks. In *Proc. IEEE Conf. Comput. Vis. Pattern Recog. (CVPR)*, pages 2414–2423, 2016. [4](#)
- [24] Yujie Hou, Jiwei Chen, and Zengfu Wang. Multi-branch network with ensemble learning for text removal in the wild. In *Proc. Asian Conf. Comput. Vis. (ACCV)*, pages 1333–1349, 2022. [2](#), [6](#)
- [25] Liufeng Huang, Bangdong Chen, Chongyu Liu, Dezhi Peng, Weiyang Zhou, Yaqiang Wu, Hui Li, Hao Ni, and Lianwen Jin. EnsExam: A dataset for handwritten text era-

- sure on examination papers. In *Proc. Int. Conf. Doc. Anal. Recognit. (ICDAR)*, pages 470–485, 2023. [1](#)
- [26] Mingxin Huang, Jiabin Zhang, Dezhi Peng, Hao Lu, Can Huang, Yuliang Liu, Xiang Bai, and Lianwen Jin. ES-TextSpotter: Towards better scene text spotting with explicit synergy in Transformer. In *Proc. Int. Conf. Comput. Vis. (ICCV)*, pages 19495–19505, 2023. [3](#)
- [27] Phillip Isola, Jun-Yan Zhu, Tinghui Zhou, and Alexei A Efros. Image-to-image translation with conditional adversarial networks. In *Proc. IEEE Conf. Comput. Vis. Pattern Recog. (CVPR)*, pages 1125–1134, 2017. [2](#), [6](#)
- [28] Andrew Jaegle, Felix Gimeno, Andy Brock, Oriol Vinyals, Andrew Zisserman, and Joao Carreira. Perceiver: General perception with iterative attention. In *Proc. Int. Conf. Mach. Learn. (ICML)*, pages 4651–4664, 2021. [3](#)
- [29] Andrew Jaegle, Sebastian Borgeaud, Jean-Baptiste Alayrac, Carl Doersch, Catalin Ionescu, David Ding, Skanda Koppula, Daniel Zoran, Andrew Brock, Evan Shelhamer, et al. Perceiver IO: A general architecture for structured inputs & outputs. In *Proc. Int. Conf. Learn. Represent. (ICLR)*, 2022. [3](#)
- [30] Gangwei Jiang, Shiyao Wang, Tiezheng Ge, Yuning Jiang, Ying Wei, and Defu Lian. Self-supervised text erasing with controllable image synthesis. In *Proc. ACM Int. Conf. Multimedia (ACM MM)*, pages 1973–1983, 2022. [2](#)
- [31] Justin Johnson, Alexandre Alahi, and Li Fei-Fei. Perceptual losses for real-time style transfer and super-resolution. In *Proc. Eur. Conf. Comput. Vis. (ECCV)*, pages 694–711, 2016. [4](#)
- [32] Prateek Keserwani and Partha Pratim Roy. Text region conditional generative adversarial network for text concealment in the wild. *IEEE Trans. Circuits Syst. Video Technol.*, 32(5):3152–3163, 2021. [2](#)
- [33] Geewook Kim, Teakgyu Hong, Moonbin Yim, JeongYeon Nam, Jinyoung Park, Jinyeong Yim, Wonseok Hwang, Sangdoon Yun, Dongyoon Han, and Seunghyun Park. OCR-free document understanding Transformer. In *Proc. Eur. Conf. Comput. Vis. (ECCV)*, pages 498–517, 2022. [2](#), [3](#), [4](#)
- [34] Myung-Joon Kwon, In-Jae Yu, Seung-Hun Nam, and Heung-Kyu Lee. CAT-Net: Compression artifact tracing network for detection and localization of image splicing. In *Proc. IEEE Winter Conf. Appl. Comput. Vis. (WACV)*, pages 375–384, 2021. [3](#)
- [35] Myung-Joon Kwon, Seung-Hun Nam, In-Jae Yu, Heung-Kyu Lee, and Changick Kim. Learning JPEG compression artifacts for image manipulation detection and localization. *Int. J. Comput. Vis.*, 130(8):1875–1895, 2022. [3](#), [7](#), [8](#), [19](#)
- [36] Hyeonsu Lee and Chankyu Choi. The surprisingly straightforward scene text removal method with gated attention and region of interest generation: A comprehensive prominent model analysis. In *Proc. Eur. Conf. Comput. Vis. (ECCV)*, pages 457–472, 2022. [1](#), [2](#), [6](#), [18](#)
- [37] Bohan Li, Ye Yuan, Dingkan Liang, Xiao Liu, Zhilong Ji, Jinfeng Bai, Wenyu Liu, and Xiang Bai. When counting meets HMER: Counting-aware network for handwritten mathematical expression recognition. In *Proc. Eur. Conf. Comput. Vis. (ECCV)*, pages 197–214, 2022. [1](#)
- [38] Junnan Li, Dongxu Li, Silvio Savarese, and Steven Hoi. BLIP-2: Bootstrapping language-image pre-training with frozen image encoders and large language models. In *Proc. Int. Conf. Mach. Learn. (ICML)*, 2023. [2](#), [3](#), [5](#)
- [39] Minghui Liao, Guan Pang, Jing Huang, Tal Hassner, and Xiang Bai. Mask TextSpotter v3: Segmentation proposal network for robust scene text spotting. In *Proc. Eur. Conf. Comput. Vis. (ECCV)*, pages 706–722, 2020. [1](#)
- [40] Chongyu Liu, Yuliang Liu, Lianwen Jin, Shuaitao Zhang, Canjie Luo, and Yongpan Wang. EraseNet: End-to-end text removal in the wild. *IEEE Trans. Image Process.*, 29:8760–8775, 2020. [1](#), [2](#), [4](#), [5](#), [6](#), [7](#), [14](#), [18](#)
- [41] Chongyu Liu, Lianwen Jin, Yuliang Liu, Canjie Luo, Bangdong Chen, Fengjun Guo, and Kai Ding. Don’t forget me: Accurate background recovery for text removal via modeling local-global context. In *Proc. Eur. Conf. Comput. Vis. (ECCV)*, pages 409–426, 2022. [1](#), [2](#), [4](#), [5](#), [6](#), [14](#), [18](#)
- [42] Haotian Liu, Chunyuan Li, Qingyang Wu, and Yong Jae Lee. Visual instruction tuning. *arXiv preprint arXiv:2304.08485*, 2023. [2](#), [3](#), [5](#)
- [43] Yuliang Liu, Hao Chen, Chunhua Shen, Tong He, Lianwen Jin, and Liangwei Wang. ABCNet: Real-time scene text spotting with adaptive bezier-curve network. In *Proc. IEEE Conf. Comput. Vis. Pattern Recog. (CVPR)*, pages 9809–9818, 2020. [1](#)
- [44] Yuliang Liu, Zhang Li, Hongliang Li, Wenwen Yu, Mingxin Huang, Dezhi Peng, Mingyu Liu, Mingrui Chen, Chunyuan Li, Lianwen Jin, et al. On the hidden mystery of OCR in large multimodal models. *arXiv preprint arXiv:2305.07895*, 2023. [2](#)
- [45] Yuliang Liu, Jiabin Zhang, Dezhi Peng, Mingxin Huang, Xinyu Wang, Jingqun Tang, Can Huang, Dahua Lin, Chunhua Shen, Xiang Bai, and Lianwen Jin. SPTS v2: Single-point scene text spotting. *IEEE Trans. Pattern Anal. Mach. Intell.*, 45(12):15665–15679, 2023. [3](#)
- [46] Ze Liu, Yutong Lin, Yue Cao, Han Hu, Yixuan Wei, Zheng Zhang, Stephen Lin, and Baining Guo. Swin Transformer: Hierarchical vision Transformer using shifted windows. In *Proc. Int. Conf. Comput. Vis. (ICCV)*, pages 10012–10022, 2021. [7](#), [19](#)
- [47] Ze Liu, Han Hu, Yutong Lin, Zhuliang Yao, Zhenda Xie, Yixuan Wei, Jia Ning, Yue Cao, Zheng Zhang, Li Dong, et al. Swin Transformer v2: Scaling up capacity and resolution. In *Proc. IEEE Conf. Comput. Vis. Pattern Recog. (CVPR)*, pages 12009–12019, 2022. [4](#), [5](#), [13](#)
- [48] Ilya Loshchilov and Frank Hutter. Decoupled weight decay regularization. In *Proc. Int. Conf. Learn. Represent. (ICLR)*, 2019. [14](#)
- [49] Jiasen Lu, Christopher Clark, Rowan Zellers, Roozbeh Mottaghi, and Aniruddha Kembhavi. Unified-IO: A unified model for vision, language, and multi-modal tasks. In *Proc. Int. Conf. Learn. Represent. (ICLR)*, 2022. [2](#), [3](#), [15](#)
- [50] Dongliang Luo, Yu Zhou, Rui Yang, Yuliang Liu, Xianjin Liu, Jishen Zeng, Enming Zhang, Biao Yang, Ziming Huang, Lianwen Jin, et al. ICDAR 2023 competition on detecting tampered text in images. In *Proc. Int. Conf. Doc. Anal. Recognit. (ICDAR)*, pages 587–600, 2023. [1](#)

- [51] Tengchao Lv, Yupan Huang, Jingye Chen, Lei Cui, Shuming Ma, Yaoyao Chang, Shaohan Huang, Wenhui Wang, Li Dong, Weiyao Luo, et al. Kosmos-2.5: A multimodal literature model. *arXiv preprint arXiv:2309.11419*, 2023. [2](#), [3](#), [4](#), [5](#)
- [52] Guangtao Lyu and Anna Zhu. PSSTRNet: Progressive segmentation-guided scene text removal network. In *Proc. Int. Conf. Multimedia and Expo (ICME)*, pages 1–6, 2022. [2](#), [3](#), [6](#)
- [53] Guangtao Lyu, Kun Liu, Anna Zhu, Seiichi Uchida, and Brian Kenji Iwana. FETNet: Feature erasing and transferring network for scene text removal. *Pattern Recognit.*, page 109531, 2023. [2](#), [6](#)
- [54] Mehdi Mirza and Simon Osindero. Conditional generative adversarial nets. *arXiv preprint arXiv:1411.1784*, 2014. [2](#)
- [55] Toshiaki Nakamura, Anna Zhu, Keiji Yanai, and Seiichi Uchida. Scene text eraser. In *Proc. Int. Conf. Doc. Anal. Recognit. (ICDAR)*, pages 832–837, 2017. [1](#), [2](#), [6](#)
- [56] OpenAI. GPT-4 technical report, 2023. [3](#)
- [57] Dezhi Peng, Lianwen Jin, Yuliang Liu, Canjie Luo, and Songxuan Lai. PageNet: Towards end-to-end weakly supervised page-level handwritten Chinese text recognition. *Int. J. Comput. Vis.*, 130(11):2623–2645, 2022. [1](#)
- [58] Dezhi Peng, Xinyu Wang, Yuliang Liu, Jiabin Zhang, Mingxin Huang, Songxuan Lai, Jing Li, Shenggao Zhu, Dahua Lin, Chunhua Shen, et al. SPTS: Single-point text spotting. In *Proc. ACM Int. Conf. Multimedia (ACM MM)*, pages 4272–4281, 2022. [3](#)
- [59] Dezhi Peng, Chongyu Liu, Yuliang Liu, and Lianwen Jin. ViTEraser: Harnessing the power of vision Transformers for scene text removal with SegMIM pretraining. *arXiv preprint arXiv:2306.12106*, 2023. [1](#), [2](#), [3](#), [4](#), [5](#), [6](#), [7](#), [14](#), [17](#)
- [60] Dezhi Peng, Weihong Ma, Canyu Xie, Hesuo Zhang, Shenggao Zhu, and Jing Li. Recognition of handwritten Chinese text by segmentation: A segment-annotation-free approach. *IEEE Trans. Multimedia*, 25:2368–2381, 2023. [1](#)
- [61] Siyang Qin, Jiahui Wei, and Roberto Manduchi. Automatic semantic content removal by learning to neglect. In *Proc. Br. Mach. Vis. Conf. (BMVC)*, pages 1–12, 2018. [2](#)
- [62] Chenfan Qu, Chongyu Liu, Yuliang Liu, Xinhong Chen, Dezhi Peng, Fengjun Guo, and Lianwen Jin. Towards robust tampered text detection in document image: New dataset and new solution. In *Proc. IEEE Conf. Comput. Vis. Pattern Recog. (CVPR)*, pages 5937–5946, 2023. [1](#), [2](#), [3](#), [8](#)
- [63] Yujin Ren, Jiabin Zhang, Bangdong Chen, Xiaoyi Zhang, and Lianwen Jin. Looking from a higher-level perspective: Attention and recognition enhanced multi-scale scene text segmentation. In *Proc. Asian Conf. Comput. Vis. (ACCV)*, pages 3138–3154, 2022. [1](#), [2](#), [3](#), [6](#), [18](#)
- [64] Olaf Ronneberger, Philipp Fischer, and Thomas Brox. U-Net: Convolutional networks for biomedical image segmentation. In *Proc. Int. Conf. Med. Image Comput. Comput.-Assisted Intervention (MICCAI)*, pages 234–241, 2015. [6](#), [18](#)
- [65] Yongxin Shi, Dezhi Peng, Wenhui Liao, Zening Lin, Xinhong Chen, Chongyu Liu, Yuyi Zhang, and Lianwen Jin. Exploring OCR capabilities of GPT-4V (ision): A quantitative and in-depth evaluation. *arXiv preprint arXiv:2310.16809*, 2023. [2](#)
- [66] Karen Simonyan and Andrew Zisserman. Very deep convolutional networks for large-scale image recognition. In *Proc. Int. Conf. Learn. Represent. (ICLR)*, 2015. [4](#), [14](#)
- [67] Zhengmi Tang, Tomo Miyazaki, Yoshihiro Sugaya, and Shinichiro Omachi. Stroke-based scene text erasing using synthetic data for training. *IEEE Trans. Image Process.*, 30: 9306–9320, 2021. [2](#), [6](#), [18](#)
- [68] Zineng Tang, Ziyi Yang, Guoxin Wang, Yuwei Fang, Yang Liu, Chenguang Zhu, Michael Zeng, Cha Zhang, and Mohit Bansal. Unifying vision, text, and layout for universal document processing. In *Proc. IEEE Conf. Comput. Vis. Pattern Recog. (CVPR)*, pages 19254–19264, 2023. [2](#), [3](#), [4](#)
- [69] Hugo Touvron, Thibaut Lavril, Gautier Izacard, Xavier Martinet, Marie-Anne Lachaux, Timothée Lacroix, Baptiste Rozière, Naman Goyal, Eric Hambro, Faisal Azhar, et al. LLaMA: Open and efficient foundation language models. *arXiv preprint arXiv:2302.13971*, 2023. [2](#), [3](#)
- [70] Osman Tursun, Rui Zeng, Simon Denman, Sabesan Sivapalan, Sridha Sridharan, and Clinton Fookes. MTRNet: A generic scene text eraser. In *Proc. Int. Conf. Doc. Anal. Recognit. (ICDAR)*, pages 39–44, 2019. [2](#)
- [71] Osman Tursun, Simon Denman, Rui Zeng, Sabesan Sivapalan, Sridha Sridharan, and Clinton Fookes. MTRNet++: One-stage mask-based scene text eraser. *Comput. Vis. Image Underst.*, 201:103066, 2020. [1](#), [2](#), [6](#), [18](#)
- [72] Ashish Vaswani, Noam Shazeer, Niki Parmar, Jakob Uszkoreit, Llion Jones, Aidan N Gomez, Łukasz Kaiser, and Illia Polosukhin. Attention is all you need. *Proc. Adv. Neural Inf. Process. Syst. (NeurIPS)*, 30, 2017. [2](#), [3](#)
- [73] Chuan Wang, Shan Zhao, Li Zhu, Kunming Luo, Yanwen Guo, Jue Wang, and Shuaicheng Liu. Semi-supervised pixel-level scene text segmentation by mutually guided network. *IEEE Trans. Image Process.*, 30:8212–8221, 2021. [1](#), [2](#), [3](#)
- [74] Jingdong Wang, Ke Sun, Tianheng Cheng, Borui Jiang, Chaorui Deng, Yang Zhao, Dong Liu, Yadong Mu, Mingkui Tan, Xinggang Wang, et al. Deep high-resolution representation learning for visual recognition. *IEEE Trans. Pattern Anal. Mach. Intell.*, 43(10):3349–3364, 2020. [6](#), [7](#), [18](#), [19](#)
- [75] Jianfeng Wang, Zhengyuan Yang, Xiaowei Hu, Linjie Li, Kevin Lin, Zhe Gan, Zicheng Liu, Ce Liu, and Lijuan Wang. GIT: A generative image-to-text Transformer for vision and language. *Trans. on Mach. Learn. Res.*, 2022. [3](#)
- [76] Peng Wang, An Yang, Rui Men, Junyang Lin, Shuai Bai, Zhikang Li, Jianxin Ma, Chang Zhou, Jingren Zhou, and Hongxia Yang. OFA: Unifying architectures, tasks, and modalities through a simple sequence-to-sequence learning framework. In *Proc. Int. Conf. Mach. Learn. (ICML)*, pages 23318–23340, 2022. [2](#), [3](#), [15](#), [16](#)
- [77] Wenhui Wang, Enze Xie, Xiang Li, Wenbo Hou, Tong Lu, Gang Yu, and Shuai Shao. Shape robust text detection with progressive scale expansion network. In *Proc. IEEE*

- Conf. Comput. Vis. Pattern Recog. (CVPR)*, pages 9336–9345, 2019. 7
- [78] Xiaobing Wang, Yingying Jiang, Zhenbo Luo, Cheng-Lin Liu, Hyunsoo Choi, and Sungjin Kim. Arbitrary shape scene text detection with adaptive text region representation. In *Proc. IEEE Conf. Comput. Vis. Pattern Recog. (CVPR)*, pages 6449–6458, 2019. 7
- [79] Xinlong Wang, Wen Wang, Yue Cao, Chunhua Shen, and Tiejun Huang. Images speak in images: A generalist painter for in-context visual learning. In *Proc. IEEE Conf. Comput. Vis. Pattern Recog. (CVPR)*, pages 6830–6839, 2023. 2, 3, 8, 15, 16
- [80] Xiaocong Wang, Chaoyue Wu, Haiyang Yu, Bin Li, and Xiangyang Xue. TextFormer: Component-aware text segmentation with Transformer. In *Proc. Int. Conf. Multimedia and Expo (ICME)*, pages 1877–1882, 2023. 1, 2, 3
- [81] Yuxin Wang, Hongtao Xie, Zheng-Jun Zha, Mengting Xing, Zilong Fu, and Yongdong Zhang. ContourNet: Taking a further step toward accurate arbitrary-shaped scene text detection. In *Proc. IEEE Conf. Comput. Vis. Pattern Recog. (CVPR)*, pages 11753–11762, 2020. 7
- [82] Yuxin Wang, Hongtao Xie, Mengting Xing, Jing Wang, Shenggao Zhu, and Yongdong Zhang. Detecting tampered scene text in the wild. In *Proc. Eur. Conf. Comput. Vis. (ECCV)*, pages 215–232, 2022. 1, 3, 4, 5, 6, 7, 8, 14, 17
- [83] Yuxin Wang, Boqiang Zhang, Hongtao Xie, and Yongdong Zhang. Tampered text detection via RGB and frequency relationship modeling. *Chin. J. Netw. Inf. Secur.*, 8(3):29–40, 2022. 2, 3, 8
- [84] Yuxin Wang, Hongtao Xie, Zixiao Wang, Yadong Qu, and Yongdong Zhang. What is the real need for scene text removal? Exploring the background integrity and erasure exhaustivity properties. *IEEE Trans. Image Process.*, 32: 4567–4580, 2023. 1, 2, 3, 6, 18
- [85] Enze Xie, Wenhai Wang, Zhiding Yu, Anima Anandkumar, Jose M Alvarez, and Ping Luo. SegFormer: Simple and efficient design for semantic segmentation with Transformers. In *Proc. Adv. Neural Inf. Process. Syst. (NeurIPS)*, pages 12077–12090, 2021. 6, 7, 19
- [86] Xingqian Xu, Zhifei Zhang, Zhaowen Wang, Brian Price, Zhonghao Wang, and Humphrey Shi. Rethinking text segmentation: A novel dataset and a text-specific refinement approach. In *Proc. IEEE Conf. Comput. Vis. Pattern Recog. (CVPR)*, pages 12045–12055, 2021. 1, 2, 3, 5, 6, 8, 14, 18
- [87] Xixi Xu, Zhongang Qi, Jianqi Ma, Honglun Zhang, Ying Shan, and Xiaohu Qie. BTS: A bi-lingual benchmark for text segmentation in the wild. In *Proc. IEEE Conf. Comput. Vis. Pattern Recog. (CVPR)*, pages 19152–19162, 2022. 2, 3
- [88] Zhengyuan Yang, Zhe Gan, Jianfeng Wang, Xiaowei Hu, Faisal Ahmed, Zicheng Liu, Yumao Lu, and Lijuan Wang. UniTab: Unifying text and box outputs for grounded vision-language modeling. In *Proc. Eur. Conf. Comput. Vis. (ECCV)*, pages 521–539, 2022. 3
- [89] Jiabo Ye, Anwen Hu, Haiyang Xu, Qinghao Ye, Ming Yan, Yuhao Dan, Chenlin Zhao, Guohai Xu, Chenliang Li, Junfeng Tian, et al. mPLUG-DocOwl: Modularized multi-modal large language model for document understanding. *arXiv preprint arXiv:2307.02499*, 2023. 2, 3
- [90] Jiabo Ye, Anwen Hu, Haiyang Xu, Qinghao Ye, Ming Yan, Guohai Xu, Chenliang Li, Junfeng Tian, Qi Qian, Ji Zhang, et al. UReader: Universal OCR-free visually-situated language understanding with multimodal large language model. *arXiv preprint arXiv:2310.05126*, 2023. 2, 3
- [91] Qinghao Ye, Haiyang Xu, Guohai Xu, Jiabo Ye, Ming Yan, Yiyang Zhou, Junyang Wang, Anwen Hu, Pengcheng Shi, Yaya Shi, et al. mPLUG-Owl: Modularization empowers large language models with multimodality. *arXiv preprint arXiv:2304.14178*, 2023. 2, 3
- [92] Haiyang Yu, Xiaocong Wang, Ke Niu, Bin Li, and Xiangyang Xue. Scene text segmentation with text-focused Transformers. In *Proc. ACM Int. Conf. Multimedia (ACM MM)*, pages 2898–2907, 2023. 1, 2, 3, 6
- [93] Jan Zdenek and Hideki Nakayama. Erasing scene text with weak supervision. In *Proc. IEEE Winter Conf. Appl. Comput. Vis. (WACV)*, pages 2238–2246, 2020. 2
- [94] Renrui Zhang, Jiaming Han, Aojun Zhou, Xiangfei Hu, Shilin Yan, Pan Lu, Hongsheng Li, Peng Gao, and Yu Qiao. LLaMA-Adapter: Efficient fine-tuning of language models with zero-init attention. *arXiv preprint arXiv:2303.16199*, 2023. 2, 3
- [95] Shuaitao Zhang, Yulian Liu, Lianwen Jin, Yaoxiong Huang, and Songxuan Lai. EnsNet: Ensconce text in the wild. In *Proc. AAAI Conf. Artif. Intell. (AAAI)*, pages 801–808, 2019. 1, 2, 6, 14
- [96] Yiyuan Zhang, Kaixiong Gong, Kaipeng Zhang, Hongsheng Li, Yu Qiao, Wanli Ouyang, and Xiangyu Yue. Meta-Transformer: A unified framework for multimodal learning. *arXiv preprint arXiv:2307.10802*, 2023. 3
- [97] Hengshuang Zhao, Jianping Shi, Xiaojuan Qi, Xiaogang Wang, and Jiaya Jia. Pyramid scene parsing network. In *Proc. IEEE Conf. Comput. Vis. Pattern Recog. (CVPR)*, pages 2881–2890, 2017. 3
- [98] Peng Zhou, Xintong Han, Vlad I Morariu, and Larry S Davis. Learning rich features for image manipulation detection. In *Proc. IEEE Conf. Comput. Vis. Pattern Recog. (CVPR)*, pages 1053–1061, 2018. 3
- [99] Xinyu Zhou, Cong Yao, He Wen, Yuzhi Wang, Shuchang Zhou, Weiran He, and Jiajun Liang. EAST: An efficient and accurate scene text detector. In *Proc. IEEE Conf. Comput. Vis. Pattern Recog. (CVPR)*, pages 5551–5560, 2017. 7
- [100] Deyao Zhu, Jun Chen, Xiaoqian Shen, Xiang Li, and Mohamed Elhoseiny. MiniGPT-4: Enhancing vision-language understanding with advanced large language models. *arXiv preprint arXiv:2304.10592*, 2023. 2, 3, 5
- [101] Xizhou Zhu, Jinguo Zhu, Hao Li, Xiaoshi Wu, Hongsheng Li, Xiaohua Wang, and Jifeng Dai. Uni-Perceiver: Pre-training unified architecture for generic perception for zero-shot and few-shot tasks. In *Proc. IEEE Conf. Comput. Vis. Pattern Recog. (CVPR)*, pages 16804–16815, 2022. 3

A. Implementation Details

In this section, we supplement every detail to implement the proposed UPOCR, which may not be thoroughly specified in the main paper due to the page limit.

A.1. Network Architecture

As described in Secs. 3.2 and 4.1 of the main paper, the UPOCR employs a vision Transformer (ViT)-based encoder-decoder with learnable task prompts. The detailed network architecture of UPOCR is presented in Tab. 8 where the notations are defined as follows.

- D_i^{enc} : The downsampling ratio of the patch embedding layer in the i -th block of the encoder.
- E_i^{enc} : The output dimension of the patch embedding layer in the i -th block of the encoder.
- W_i^{enc} : The window size of the Swinv2 [47] blocks in the i -th block of the encoder.
- H_i^{enc} : The number of heads of the Swinv2 blocks in the i -th block of the encoder.
- C_i^{enc} : The feature dimension of the Swinv2 blocks in the i -th block of the encoder.
- N^{tp} : The number of task prompts which is equal to the number of tasks that the model is supposed to simultaneously deal with.
- C^{tp} : The dimension of task prompts.
- U_i^{dec} : The upsampling ratio of the patch splitting layer in the i -th block of the decoder.
- E_i^{dec} : The output dimension of the patch splitting layer in the i -th block of the decoder.
- W_i^{dec} : The window size of the Swinv2 blocks in the i -th block of the decoder.
- H_i^{dec} : The number of heads of the Swinv2 blocks in the i -th block of the decoder.
- C_i^{dec} : The feature dimension of the Swinv2 blocks in the i -th block of the decoder.

As shown in Tab. 8, supposing the shape of the input RGB image is $H \times W \times 3$, the encoder hierarchically produces features $\{f_i^{enc} \in \mathbb{R}^{\frac{H}{2^{(i+1)}} \times \frac{W}{2^{(i+1)}} \times C_i^{enc}}\}_{i=1}^4$. Then the learnable prompt of the target task is integrated into the final feature f_4^{enc} of the encoder, yielding a task-specific feature for decoding. Subsequently, the decoder hierarchically generates features $\{f_i^{dec} \in \mathbb{R}^{\frac{H}{2^{(5-i)}} \times \frac{W}{2^{(5-i)}} \times C_i^{dec}}\}_{i=1}^5$ based on the task-specific feature. Finally, the output image is predicted based on feature f_5^{dec} through a 3×3 convolution.

Task Prompt Insertion. The task prompts are formulated as a set of learnable embeddings $f^{tp} \in \mathbb{R}^{N^{tp} \times C^{tp}}$, where $N^{tp} = 3$ and $C^{tp} = 768$ are the number of tasks and embedding dimension, respectively. To perform the i -th task, the correspond prompt $f_i^{tp} \in \mathbb{R}^{1 \times 768}$ is first repeated by $\frac{H}{32} \times \frac{W}{32}$ times, yielding a feature $\hat{f}_i^{tp} \in \mathbb{R}^{\frac{H}{32} \times \frac{W}{32} \times 768}$. Then the \hat{f}_i^{tp} is element-wise added to the final feature $f_4^{enc} \in \mathbb{R}^{\frac{H}{32} \times \frac{W}{32} \times 768}$ of the encoder, pushing the general

	Block	Output Size	Layer Name	Details
Encoder	Block 1	$\frac{H}{4} \times \frac{W}{4}$	Patch Embedding	$D_1^{enc} = 4, E_1^{enc} = 96$
			Swinv2 block	$\begin{matrix} W_1^{enc} = 16 \\ H_1^{enc} = 3 \\ C_1^{enc} = 96 \end{matrix} \times 2$
	Block 2	$\frac{H}{8} \times \frac{W}{8}$	Patch Embedding	$D_2^{enc} = 2, E_2^{enc} = 192$
			Swinv2 block	$\begin{matrix} W_2^{enc} = 16 \\ H_2^{enc} = 6 \\ C_2^{enc} = 192 \end{matrix} \times 2$
	Block 3	$\frac{H}{16} \times \frac{W}{16}$	Patch Embedding	$D_3^{enc} = 2, E_3^{enc} = 384$
			Swinv2 block	$\begin{matrix} W_3^{enc} = 16 \\ H_3^{enc} = 6 \\ C_3^{enc} = 384 \end{matrix} \times 18$
	Block 4	$\frac{H}{32} \times \frac{W}{32}$	Patch Embedding	$D_4^{enc} = 2, E_4^{enc} = 768$
			Swinv2 block	$\begin{matrix} W_4^{enc} = 16 \\ H_4^{enc} = 24 \\ C_4^{enc} = 768 \end{matrix} \times 2$
Task Prompts	$\frac{H}{32} \times \frac{W}{32}$	$N^{tp} = 3, C^{tp} = 768$		
Decoder	Block 1	$\frac{H}{16} \times \frac{W}{16}$	Swinv2 block	$\begin{matrix} W_1^{dec} = 8 \\ H_1^{dec} = 24 \\ C_1^{dec} = 768 \end{matrix} \times 2$
			Patch Splitting	$U_1^{dec} = 2, E_1^{dec} = 384$
	Block 2	$\frac{H}{8} \times \frac{W}{8}$	Swinv2 block	$\begin{matrix} W_2^{dec} = 8 \\ H_2^{dec} = 12 \\ C_2^{dec} = 384 \end{matrix} \times 18$
			Patch Splitting	$U_2^{dec} = 2, E_2^{dec} = 192$
	Block 3	$\frac{H}{4} \times \frac{W}{4}$	Swinv2 block	$\begin{matrix} W_3^{dec} = 8 \\ H_3^{dec} = 6 \\ C_3^{dec} = 192 \end{matrix} \times 2$
			Patch Splitting	$U_3^{dec} = 2, E_3^{dec} = 96$
	Block 4	$\frac{H}{2} \times \frac{W}{2}$	Swinv2 block	$\begin{matrix} W_4^{dec} = 8 \\ H_4^{dec} = 3 \\ C_4^{dec} = 96 \end{matrix} \times 2$
			Patch Splitting	$U_4^{dec} = 2, E_4^{dec} = 48$
	Block 5	$H \times W$	Swinv2 block	$\begin{matrix} W_5^{dec} = 8 \\ H_5^{dec} = 2 \\ C_5^{dec} = 48 \end{matrix} \times 2$
			Patch Splitting	$U_5^{dec} = 2, E_5^{dec} = 24$

Table 8. Detailed network architecture of the proposed UPOCR.

representations toward task-specific regions.

Patch Embedding. Given an input feature map or image $f_{in} \in \mathbb{R}^{h \times w \times c_{in}}$, a patch embedding layer with a downsampling ratio of r and an output dimension of c_{out} first flattens each $r \times r$ patch, yield an intermediate feature $f' \in \mathbb{R}^{\frac{h}{r} \times \frac{w}{r} \times r^2 c_{in}}$. Then a linear layer is adopted to transform the dimension of feature f' , producing the output feature $f_{out} \in \mathbb{R}^{\frac{h}{r} \times \frac{w}{r} \times c_{out}}$.

Patch Splitting. Supposing the input feature is $f_{in} \in \mathbb{R}^{h \times w \times c_{in}}$, a patch splitting layer with r upsampling ratio and c_{out} output dimension first generates an intermediate feature $f' \in \mathbb{R}^{r h \times r w \times \frac{c_{in}}{r^2}}$ by decomposing each pixel of the input feature into a $r \times r$ patch. Subsequently, the feature f' goes through a linear layer to transform the feature dimension, yielding the output feature $f_{out} \in \mathbb{R}^{r h \times r w \times c_{out}}$.

Lateral Connection. As shown in Fig. 2(b) of the main paper, lateral connections are built between the encoder and decoder blocks to shortcut the transmission of fine-grained representations. Specifically, the encoder features $\{f_i^{enc}\}_{i=1}^3$ are laterally connected to the decoder features

$\{f_{4-i}^{dec}\}_{i=1}^3$. As for the architecture, if the feature $f_1 \in \mathbb{R}^{h \times w \times c}$ is connected to feature $f_2 \in \mathbb{R}^{h \times w \times c}$, the lateral connection processes the feature f_1 sequentially using a 1×1 convolution with c channels for non-linear transformation, two 3×3 convolutions with $2c$ channels for expanding, and a 1×1 convolution with c channels for shrinking, following EraseNet [40]. Then the resulting feature is element-wise added to feature f_2 .

A.2. Loss Function

Pixel Space. As described in Sec. 3.3 and defined in Eq. (1) of the main paper, the pixel loss is formulated as the weighted sum of L1 distances between multi-scale output images $\mathbb{I}_{out} = \{I_{out}^{\frac{1}{4}}, I_{out}^{\frac{1}{2}}, I_{out}\}$ and ground-truth (GT) images $\mathbb{I}_{gt} = \{I_{gt}^{\frac{1}{4}}, I_{gt}^{\frac{1}{2}}, I_{gt}\}$.

In practical implementation, for samples of the text removal task, the GT text box mask M_{gt} is incorporated to focus more on the discrepancy in text regions, following most existing text removal methods [40, 41, 95]. Specifically, the $M_{gt} \in \mathbb{R}^{H \times W}$ is a binary mask at the bounding-box level where 1 and 0 values indicate text and non-text pixels, respectively. Similar to \mathbb{I}_{gt} , we also resize M_{gt} to multiple scales denoted as $\mathbb{M}_{gt} = \{M_{gt}^{\frac{1}{4}}, M_{gt}^{\frac{1}{2}}, M_{gt}\}$. Then the pixel loss of text removal samples is calculated as

$$L_{pix}^{tr} = \sum_{i=1}^3 \alpha_i \|(\mathbb{I}_{out(i)} - \mathbb{I}_{gt(i)}) \odot \mathbb{M}_{gt(i)}\|_1 + \beta_i \|(\mathbb{I}_{out(i)} - \mathbb{I}_{gt(i)}) \odot (1 - \mathbb{M}_{gt(i)})\|_1, \quad (4)$$

where α and β are empirically set to $\{5, 6, 10\}$ (as specified in Sec. 3.3 of the main paper) and $\{0.8, 1, 2\}$, respectively.

As for the text segmentation and tampered text detection tasks, smooth L1 loss functions are employed in Eq. (1) of the main paper to replace the standard L1 distance, because it is not required to precisely align the pixel values of output and GT images but critical to penalize the outliers for these two segmentation-oriented tasks.

Feature Space. As specified in Sec. 3.3 and Eq. (2) of the main paper, a feature loss L_{feat} containing perceptual loss L_{per} and style loss L_{sty} is adopted to ensure the visual plausibility of generated images. Concretely, the losses L_{per} and L_{sty} are formulated as

$$I_{out}^* = I_{out} \odot M_{gt} + I_{in} \odot (1 - M_{gt}), \quad (5)$$

$$L_{per} = \sum_{i=1}^3 \|\Phi_i(I_{out}) - \Phi_i(I_{gt})\|_1 + \|\Phi(I_{out}^*) - \Phi(I_{gt})\|_1, \quad (6)$$

$$L_{sty} = \sum_{i=1}^3 \|Gram(\Phi_i(I_{out})) - Gram(\Phi_i(I_{gt}))\|_1 + \|Gram(\Phi_i(I_{out}^*)) - Gram(\Phi_i(I_{gt}))\|_1, \quad (7)$$

where I_{in} is the input image and $Gram(\cdot)$ calculates the Gram matrix of the input feature map. Moreover, the $\Phi_i(x)$

represents the feature map produced by the i -th pooling layer of an ImageNet [16]-pretrained VGG-16 [66] network fed with an input x .

A.3. Dataset Statistics

As described in Sec. 4.1 of the main paper, experiments are conducted using the SCUT-EnsText [40], TextSeg [86], and Tampered-IC13 [82] datasets for the text removal, text segmentation, and tampered text detection tasks, respectively. The statistics of these datasets are introduced as follows.

SCUT-EnsText is a real-world scene text removal dataset, comprising 2,749 samples for training and 813 samples for testing.

TextSeg is a large-scale fine-annotated text segmentation dataset with 4,024 images of scene text and design text. The training, validating, and testing sets contain 2,646, 340, and 1,038 samples, respectively.

Tampered-IC13 is aimed at tampered scene text detection in the wild. The dataset is divided into 229 training samples and 233 testing samples. The annotation includes bounding boxes of real and tampered texts.

A.4. Training Setting

The proposed UPOCR is implemented with PyTorch³. During training, the parameters of UPOCR are initialized using the pretrained ViTEraser-Small weights (with SegMIM pre-training) [59]. Subsequently, the model is optimized for 80,000 iterations with a batch size of 48 using an AdamW [48] optimizer. Specifically, each batch consists of 16 samples from SCUT-EnsText [40] for text removal, 16 samples from TextSeg [86] for text segmentation, and 16 samples from Tampered-IC13 [82] for tampered text detection. The size of training images is set to 512×512 . The learning rate is initialized as 0.0005 and linearly decays per 200 iterations, finally reaching 0.00001 at the last 200 iterations. The training lasts approximately 36 hours using two NVIDIA A100 GPUs with 80GB memory.

A.5. Inference

In this section, we detail the inference procedure mentioned in Sec. 3.1 of the main paper. For instance, given an input image $I_{in} \in \mathbb{R}^{H \times W \times 3}$, the UPOCR produces an output image $I_{out} \in \mathbb{R}^{H \times W \times 3}$. In the following, we introduce how to obtain the formatted prediction for individual tasks from the I_{out} in detail.

Text Removal. The output image I_{out} is exactly the text-erased image without additional processing.

Text Segmentation. As we define the RGB values of foreground and background pixels as $(255, 255, 255)$ and $(0, 0, 0)$, the text-stroke pixels are determined by setting a threshold of the distance between corresponding RGB values and $(255, 255, 255)$. To achieve this efficiently, we first

³<https://pytorch.org/>

Image Size	Seq. Len.	Text Removal							Text Segmentation		Tampered Text Det.	
		PSNR \uparrow	MSSIM \uparrow	MSE \downarrow	AGE \downarrow	pEPs \downarrow	pCEPs \downarrow	FID \downarrow	fgIoU \uparrow	F \uparrow	mIoU \uparrow	mF \uparrow
512 \times 512	4096	<u>24.94</u>	<u>78.95</u>	<u>0.4871</u>	<u>8.74</u>	<u>0.1013</u>	<u>0.0125</u>	<u>19.81</u>	92.97	96.36	96.23	98.07
256 \times 256	1024	24.50	72.88	0.5110	9.43	0.1227	0.0286	41.24	84.15	91.39	<u>94.98</u>	<u>97.42</u>
UPOCR		37.14	97.62	0.0428	1.72	0.0064	0.0034	10.47	<u>88.76</u>	<u>94.04</u>	71.71	83.53

Table 9. Upper bound of OFA performance on three pixel-level OCR tasks. The performance of the proposed UPOCR is also provided for comparison, which has already significantly surpassed the upper bound of OFA on text removal. The **bold** and underline indicate the best and the second best, respectively. (Seq. Len.: Sequence Length)

normalize I_{out} to the range of $[0, 1]$ and then average the three channels, yielding $\hat{I}_{out} \in \mathbb{R}^{H \times W}$. Then the pixel at (i, j) position is identified as the text stroke if $\hat{I}_{out}^{(i,j)} > 0.4$ and the background otherwise.

Tampered Text Detection. As described in Sec. 3.1 of the main paper, we compare the distance of the generated RGB values to $(255, 0, 0)$ (red for tamper texts), $(0, 255, 0)$ (green for real texts), and $(0, 0, 255)$ (blue for backgrounds) to determine per-pixel categories. In practical implementation, it is equivalent to finding the color with the maximum value in the RGB triplet and assigning the corresponding category to the pixel, getting rid of the complex calculation of distances.

B. Further Comparison with Generalist Model

In Sec. 4.5 and Tab. 7 of the main paper, we compare the proposed UPOCR with the cutting-edge generalist model (*i.e.*, Painter [79]) that is based on image-to-image paradigms. However, existing generalist models [49, 76] with sequence-to-sequence paradigms are also able to perform image-to-image translation. For instance, given an input image, OFA [76] produces a sequence composed of discrete tokens from the VQGAN [21] codebook. After that, the output image is reconstructed from the generated sequence through the decoder of VQGAN. In this way, the OFA accomplishes the image-to-image transformation in a sequence-to-sequence manner. Therefore, based on the OFA model, we further conduct experiments and in-depth analyses to verify the effectiveness of sequence-to-sequence generalist models on pixel-level OCR tasks.

Upper Bound of OFA Performance. As described above, OFA relies on the VQGAN decoder to reconstruct the output image. However, there has already been information loss in the encoding and decoding process of VQGAN, limiting the upper bound of OFA performance. To quantify the information loss, we use VQGAN to encode the GT image I_{gt} into a sequence S_{gt} comprising discrete tokens from the codebook and then directly decode an image I_{dec} from the S_{gt} . Because the OFA is optimized to predict the sequence S_{gt} from the input image, the metrics computed using I_{dec} are the upper bound of OFA performance.

In Tab. 9, we present the upper bounds with two sizes

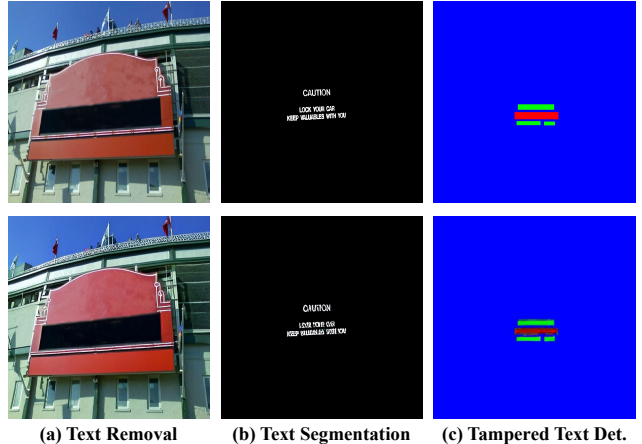


Figure 6. Visualization of GT images (top) and corresponding reconstructed results (bottom) by VQGAN. The image size is 512 \times 512. Zoom in for a better view.

of GT images, including 256 \times 256 and 512 \times 512. Using the VQGAN with a factor of 8 adopted by the OFA, they are encoded into 1024- and 4096-token sequences, respectively. The metrics listed in Tab. 9 demonstrate that the encoding and decoding procedure based on VQGAN itself has caused severe information loss. Especially for the text removal task, the proposed UPOCR has already significantly outperformed the upper bound of OFA. The reason may be that the decoder of VQGAN cannot reconstruct the details and complex patterns and also struggles to guarantee color consistency as illustrated in Fig. 6.

Comparison with OFA. Because of the overwhelming computational costs required to train an OFA with a sequence length of 4096, we set the size of input and output images to 256 \times 256 following the original configuration of OFA. Tab. 10 presents the comparison between UPOCR and different scales of OFA. Moreover, the visualizations are shown in Fig. 7. Limited by the intrinsic sequence-to-sequence mechanism, OFA exhibits significantly inferior performance on all three pixel-level OCR tasks that require strong image-to-image translation capacity. **(1) Text Removal:** As the model size increases, the OFA tends to cause larger color deviation and miss more



Figure 7. Qualitative comparison of different scales of OFA with UPOCR on (a)-(b) text removal, (c)-(d) text segmentation, and (e)-(f) tampered text detection. Zoom in for a better view.

Method	Venue	Text Removal							Text Segmentation		Tampered Text Det.		Params↓
		PSNR↑	MSSIM↑	MSE↓	AGE↓	pEPs↓	pCEPs↓	FID↓	fgIoU↑	F↑	mIoU↑	mF↑	
Sequence-to-Sequence-Based Generalist Model													
OFA _{tiny} [76]	ICML'22	20.07	67.34	1.2419	15.86	0.2262	0.1038	68.46	48.40	65.23	14.70	25.17	33M
OFA _{medium} [76]	ICML'22	19.13	62.38	1.4990	18.06	0.2639	0.1354	88.05	38.51	55.61	10.19	17.86	93M
OFA _{base} [76]	ICML'22	19.45	64.73	1.3994	16.88	0.2430	0.1172	78.85	47.77	64.66	6.34	11.90	182M
OFA _{large} [76]	ICML'22	16.04	58.08	3.0576	20.93	0.3115	0.1791	119.82	30.26	46.46	6.07	11.41	472M
OFA _{huge} [76]	ICML'22	15.73	55.80	3.2342	22.27	0.3351	0.1993	134.73	27.75	43.44	3.78	7.25	930M
Image-to-Image-Based Generalist Model													
Painter [79]	CVPR'23	<u>27.13</u>	<u>91.67</u>	<u>0.2942</u>	<u>8.68</u>	<u>0.0898</u>	<u>0.0425</u>	<u>21.90</u>	<u>86.36</u>	<u>92.68</u>	<u>69.26</u>	<u>81.83</u>	371M
UPOCR (Ours)	-	37.14	97.62	0.0428	1.72	0.0064	0.0034	10.47	88.76	94.04	71.71	83.53	108M

Table 10. Comparison with generalist models on pixel-level OCR tasks. (Params: Parameters)

details of the input image as shown in Fig. 7(a)-(b), leading to decreasing evaluation metrics. **(2) Text Segmentation:** As shown in Fig. 7(c)-(d), OFA struggles to generate the complex patterns of texts at the stroke level, primarily limited by the reconstruction capacity of the VQGAN decoder. Moreover, as the network goes deeper, the less fine-grained alignment with the input image can be guaranteed. It can be seen that OFA_{huge} just draws text-like but meaningless pat-

terns. **(3) Tampered Text Detection:** With the indirect supervision of token sequences with condensed information, OFA can hardly distinguish the inconspicuous difference between real and tampered texts, resulting in significantly poor performance on tampered text detection (Tab. 10). Moreover, the OFA is likely to produce visually plausible patches of red and green colors, ignoring the real text distribution of the input image, as shown in Fig. 7(e)-(f). Fi-

Model Size	Text Removal						Text Segmentation		Tampered Text Det.		Params↓	
	PSNR↑	MSSIM↑	MSE↓	AGE↓	pEPs↓	pCEPs↓	FID↓	fgIoU↑	F↑	mIoU↑		mF↑
UPOCR-Tiny	36.87	<u>97.59</u>	<u>0.0430</u>	1.77	<u>0.0065</u>	0.0034	10.60	<u>87.33</u>	<u>93.23</u>	68.84	81.54	65M
UPOCR-Small	<u>37.14</u>	97.62	0.0428	1.72	0.0064	0.0034	10.47	88.76	94.04	71.71	83.53	<u>108M</u>
UPOCR-Base	37.16	97.62	0.0451	1.68	0.0066	<u>0.0035</u>	<u>10.54</u>	87.20	93.16	72.95	84.36	192M

Table 11. Ablation study on different model sizes. (Params: Parameters)

nally, it is worth noting that the proposed UPOCR substantially outperforms existing generalist approaches based on either sequence-to-sequence or image-to-image paradigms, demonstrating its remarkable effectiveness and promising future in building unified pixel-level OCR interfaces.

Training Details of Painter and OFA. Following the training setting of UPOCR as specified in Sec. A.4, the Painter (Sec. 4.5 of the main paper) and OFA are trained for 80,000 iterations with a batch size of 48. Moreover, the text removal, text segmentation, and tampered text detection tasks each occupy 16 samples of a batch. Other training settings are kept the same as their original implementations.

C. Ablation Study on Model Size

As described in Sec. 4.1 of the main paper, the encoder-decoder architecture of UPOCR inherits from ViTEraser-Small [59]. In Tab. 11, we further investigate the effect of model size on the generalist capabilities of UPOCR. In addition to UPOCR (denoted as UPOCR-Small for clarity), we build UPOCR-Tiny and UPOCR-Base following the encoder-decoder architectures of ViTEraser-Tiny and ViTEraser-Base, respectively. The UPOCR-Tiny and UPOCR-Base are trained following the same setting as UPOCR and also use the weights of corresponding ViTEraser as initialization. It can be seen that UPOCR-Small significantly outperforms UPOCR-Tiny on all three tasks. However, UPOCR-Base with a larger model size exhibits inferior performance than UPOCR-Small on text segmentation and most metrics of text removal, probably due to insufficient training samples. Therefore, we opt for UPOCR-Small as the final implementation of the proposed UPOCR.

D. Limitation

Despite the effectiveness of the proposed UPOCR as a unified pixel-level OCR interface, the limitation lies in the generalization ability to unseen tasks. Although the learnable task prompts empower the UPOCR to simultaneously handle multiple tasks, they are fixed once the model training is finished, which means re-training is necessary if the pre-set range of tasks is expanded. Since task prompts function as feature-level offsets that push general representations to task-specific spaces, the automatic learning of prompts from example input-output pairs of new tasks is critical to a flexi-

ble generalist pixel-level OCR model, which is worth studying in future work.

E. More Visualization

In this section, we provide more qualitative results on text removal, text segmentation, and tampered text detection tasks in Figs. 8, 9, and 10, respectively. It can be seen that the proposed UPOCR simultaneously excels in multiple tasks with a unified single model.

Moreover, in addition to Fig. 5 of the main paper, we supplement more visualizations of three-task outputs using the test set of Tampered-IC13 [82] in Fig. 11. Specifically, all tasks are conducted with a single UPOCR model using corresponding task prompts. As demonstrated by the visualizations, UPOCR can effectively perform diverse tasks on the same input image, indicating the proposed learnable task prompts adequately guide the generation process of the decoder.



Figure 8. More visualizations on text removal, where the inference results are obtained by MTRNet++ [71], EraseNet [40], SSTE [67], GaRNet [36], CTRNet [41], PERT [84], and UPOCR (ours). Zoom in for a better view.

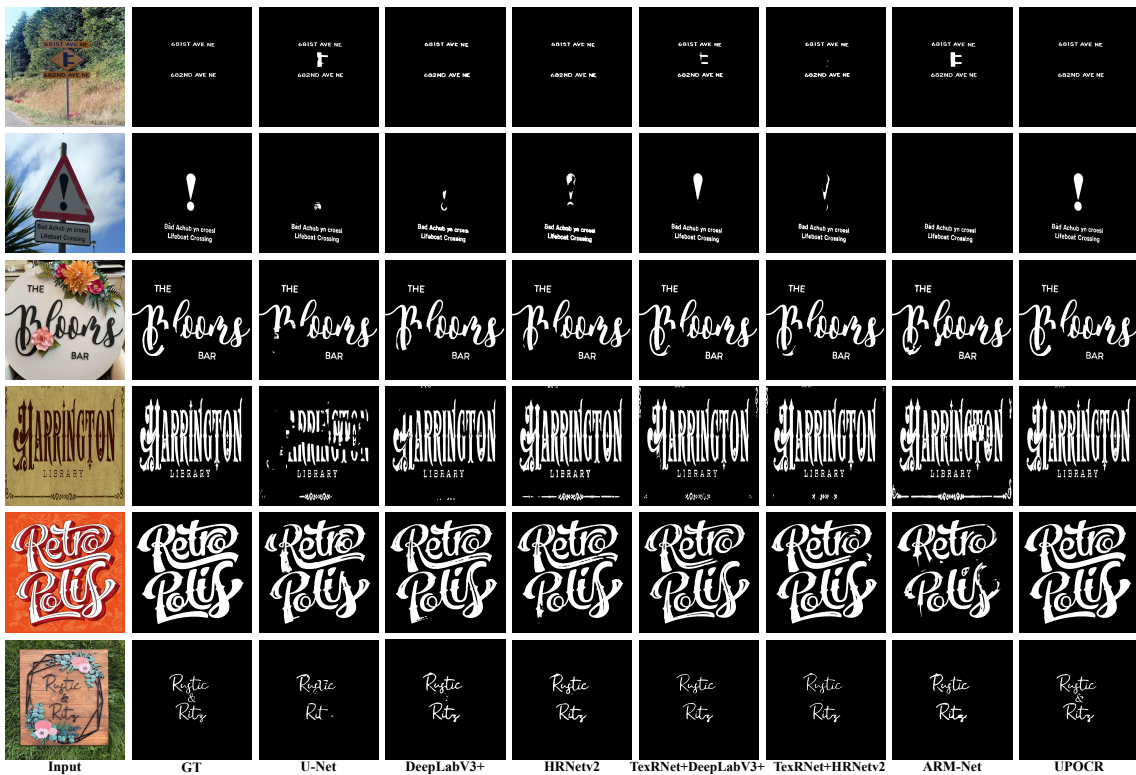


Figure 9. More visualizations on text segmentation, where the inference results are obtained by U-Net [64], DeepLabV3+ [11], HR-Netv2 [74], TexRNet+DeepLabV3+ [86], TexRNet+HRNetv2 [86], ARM-Net [63], and UPOCR (ours). Zoom in for a better view.



Figure 10. More visualizations on tampered text detection, where the inference results are obtained by DeepLabV3+ [11], HRNetv2 [74], BEiT-Uper [3], SegFormer [85], Swin-Uper [46], CAT-Net [35], and UOCR (ours). Zoom in for a better view.

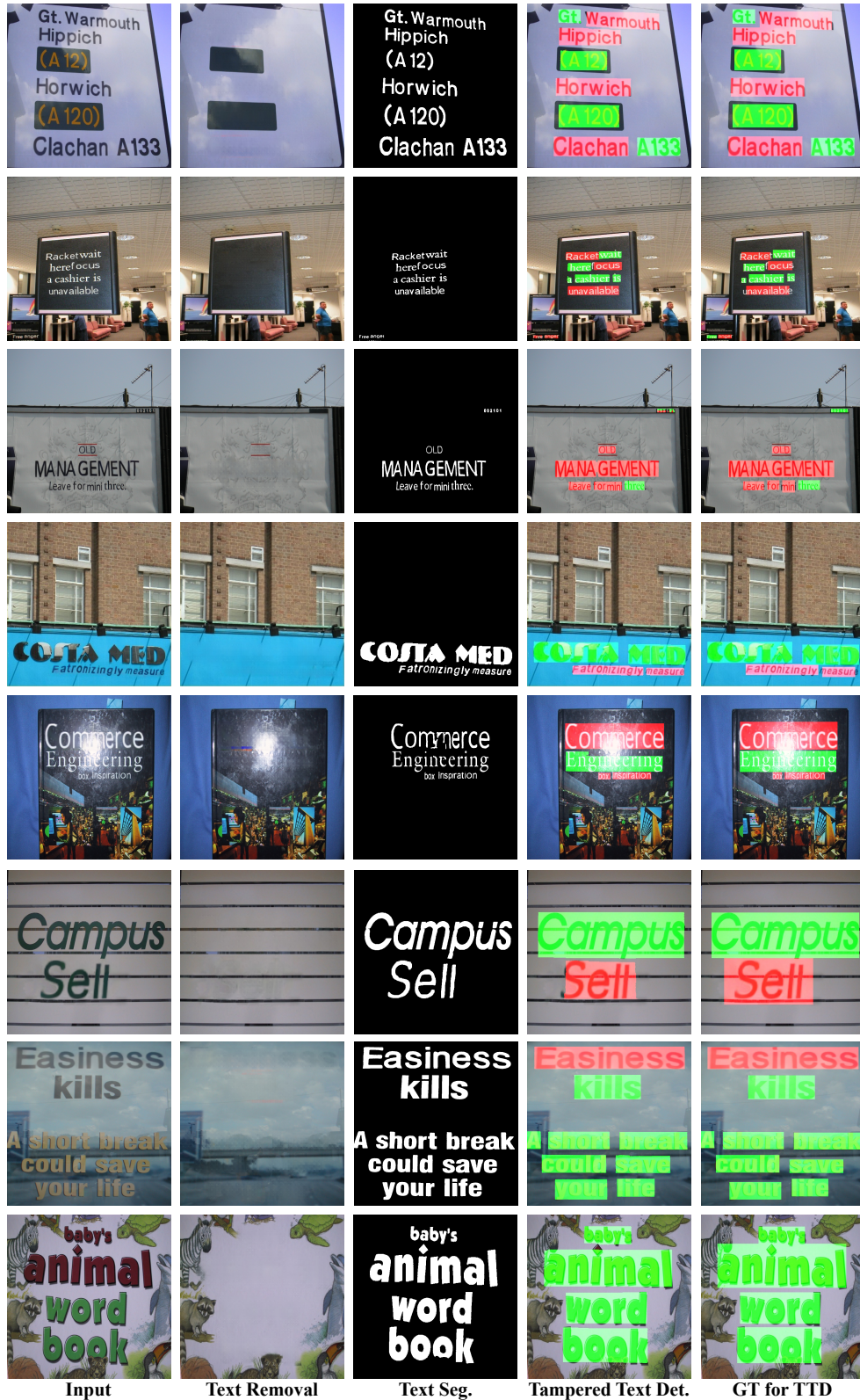


Figure 11. More visualizations of three-task outputs on Tampered-IC13 dataset. All tasks are performed with a single UPOCR model using corresponding task prompts. The GT of tampered text detection (TTD) provided by Tampered-IC13 is also presented for comparison. Zoom in for a better view. (Seg.: Segmentation, Det.: Detection)